(Research on Translational Research and Nano-medicine) from the Ministry of Health, Labor, and Welfare (Tokyo, Japan).

Disclosures

K.E. and R.M. hold a patent on the results reported in this study. The remaining authors report no conflicts.

References

1. Farber HW, Loscalzo J. Pulmonary arterial hypertension. *N Engl J Med.* 2004;351:1655–1665.
2. Humbert M, Sitbon O, Simonneau G. Treatment of pulmonary arterial hypertension. *N Engl J Med.* 2004;351:1425–1436.
3. Stenmark KR, Fagan KA, Frid MG. Hypoxia-induced pulmonary vascular remodeling: cellular and molecular mechanisms. *Circ Res.* 2006; 99:675–691.
4. Sanchez O, Marcos E, Perros F, Fadel E, Tu L, Humbert M, Dartevelle P, Simonneau G, Adnot S, Eddahibi S. Role of endothelium-derived CC chemokine ligand 2 in idiopathic pulmonary arterial hypertension. *Am J Respir Crit Care Med.* 2007;176:1041–1047.
5. Ikeda Y, Yonemitsu Y, Kataoka C, Kitamoto S, Yamaoka T, Nishida K, Takeshita A, Egashira K, Sueishi K. Anti-monocyte chemoattractant protein-1 gene therapy attenuates pulmonary hypertension in rats. *Am J Physiol Heart Circ Physiol.* 2002;283:H2021–H2028.
6. Kimura H, Kasahara Y, Kurosu K, Sugito K, Takiguchi Y, Terai M, Mikata A, Natsume M, Mukaida N, Matsushima K, Kuriyama T. Alleviation of monocrotaline-induced pulmonary hypertension by antibodies to monocyte chemotactic and activating factor/monocyte chemoattractant protein-1. *Lab Invest.* 1998;78:571–581.
7. Katsushi H, Kazufumi N, Hideki F, Katsumasa M, Hiroshi M, Kengo K, Hiroshi D, Nobuyoshi S, Tetsuro E, Hiromi M, Tohru O. Epoprostenol therapy decreases elevated circulating levels of monocyte chemoattractant protein-1 in patients with primary pulmonary hypertension. *Circ J.* 2004;68:227–231.
8. Itoh T, Nagaya N, Ishibashi-Ueda H, Kyotani S, Oya H, Sakamaki F, Kimura H, Nakanishi N. Increased plasma monocyte chemoattractant protein-1 level in idiopathic pulmonary arterial hypertension. *Respirology.* 2006;11:158–163.
9. Brand K, Page S, Rogler G, Bartsch A, Brandl R, Knuechel R, Page M, Kaltschmidt C, Baeuerle PA, Neumeier D. Activated transcription factor nuclear factor-kappa B is present in the atherosclerotic lesion. *J Clin Invest.* 1996;97:1715–1722.
10. Morishita R, Higaki J, Tomita N, Ogihara T. Application of transcription factor "decoy" strategy as means of gene therapy and study of gene expression in cardiovascular disease. *Circ Res.* 1998;82:1023–1028.
11. Kitamoto S, Egashira K, Kataoka C, Koyanagi M, Katoh M, Shimokawa H, Morishita R, Kaneda Y, Sueishi K, Takeshita A. Increased activity of nuclear factor-kappaB participates in cardiovascular remodeling induced by chronic inhibition of nitric oxide synthesis in rats. *Circulation.* 2000; 102:806–812.
12. Ohtani K, Egashira K, Nakano K, Zhao G, Funakoshi K, Ihara Y, Kimura S, Tominaga R, Morishita R, Sunagawa K. Stent-based local delivery of nuclear factor-kappaB decoy attenuates in-stent restenosis in hypercholesterolemic rabbits. *Circulation.* 2006;114:2773–2779.
13. Murakami H, Kobayashi M, Takeuchi H, Kawashima Y. Preparation of poly(DL-lactide-co-glycolide) nanoparticles by modified spontaneous emulsification solvent diffusion method. *Int J Pharm.* 1999;187:143–152.
14. Kawashima Y, Yamamoto H, Takeuchi H, Hino T, Niwa T. Properties of a peptide containing DL-lactide/glycolide copolymer nanospheres prepared by novel emulsion solvent diffusion methods. *Eur J Pharm Biopharm.* 1998;45:41–48.
15. Panyam J, Zhou WZ, Prabha S, Sahoo SK, Labhasetwar V. Rapid endolysosomal escape of poly(DL-lactide-co-glycolide) nanoparticles: implications for drug and gene delivery. *FASEB J.* 2002;16:1217–1226.
16. Schermuly RT, Dony E, Ghofrani HA, Pullamsetti S, Savai R, Roth M, Sydykov A, Lai YJ, Weissmann N, Seeger W, Grimminger F. Reversal of experimental pulmonary hypertension by PDGF inhibition. *J Clin Invest.* 2005;115:2811–2821.
17. Cowan KN, Heilbut A, Humpl T, Lam C, Ito S, Rabinovitch M. Complete reversal of fatal pulmonary hypertension in rats by a serine elastase inhibitor. *Nat Med.* 2000;6:698–702.
18. Quinlan TR, Li D, Laubach VE, Shesely EG, Zhou N, Johns RA. eNOS-deficient mice show reduced pulmonary vascular proliferation and remodeling to chronic hypoxia. *Am J Physiol Lung Cell Mol Physiol.* 2000;279:L641–L650.
19. Sawada H, Mitani Y, Maruyama J, Jiang BH, Ikeyama Y, Dida FA, Yamamoto H, Imanaka-Yoshida K, Shimpo H, Mizoguchi A, Maruyama K, Komada Y. A nuclear factor-kappaB inhibitor pyrrolidine dithiocarbamate ameliorates pulmonary hypertension in rats. *Chest.* 2007;132: 1265–1274.
20. Huang J, Kaminski PM, Edwards JG, Yeh A, Wolin MS, Frishman WH, Gewitz MH, Mathew R. Pyrrolidine dithiocarbamate restores endothelial cell membrane integrity and attenuates monocrotaline-induced pulmonary artery hypertension. *Am J Physiol Lung Cell Mol Physiol.* 2008;294: L1250–L1259.
21. Egashira K. Molecular mechanisms mediating inflammation in vascular disease: special reference to monocyte chemoattractant protein-1. *Hypertension.* 2003;41:834–841.
22. Egashira K. Clinical importance of endothelial function in arteriosclerosis and ischemic heart disease. *Circ J.* 2002;66:529–533.
23. Ohtani K, Usui M, Nakano K, Kohjimoto Y, Kitajima S, Hirouchi Y, Li XH, Kitamoto S, Takeshita A, Egashira K. Antimonocyte chemoattractant protein-1 gene therapy reduces experimental in-stent restenosis in hypercholesterolemic rabbits and monkeys. *Gene Ther.* 2004;11: 1273–1282.
24. Usui M, Egashira K, Ohtani K, Kataoka C, Ishibashi M, Hiasa K, Katoh M, Zhao Q, Kitamoto S, Takeshita A. Anti-monocyte chemoattractant protein-1 gene therapy inhibits restenotic changes (neointimal hyperplasia) after balloon injury in rats and monkeys. *FASEB J.* 2002;16: 1838–1840.
25. Egashira K, Zhao Q, Kataoka C, Ohtani K, Usui M, Charo IF, Nishida K, Inoue S, Katoh M, Ichiki T, Takeshita A. Importance of monocyte chemoattractant protein-1 pathway in neointimal hyperplasia after periarterial injury in mice and monkeys. *Circ Res.* 2002;90:1167–1172.
26. Lemarie CA, Esposito B, Tedgui A, Lehoux S. Pressure-induced vascular activation of nuclear factor-kappaB: role in cell survival. *Circ Res.* 2003; 93:207–212.
27. Egashira K, Suzuki J, Ito H, Aoki M, Isobe M, Morishita R. Long-term follow up of initial clinical cases with NF-kappaB decoy oligodeoxynucleotide transfection at the site of coronary stenting. *J Gene Med.* 2008; 10:805–809.
28. Tomoda K, Ohkoshi T, Kawai Y, Nishiwaki M, Nakajima T, Makino K. Preparation and properties of inhalable nanocomposite particles: effects of the temperature at a spray-dryer inlet upon the properties of particles. *Colloids Surf B Biointerfaces.* 2008;61:138–144.

Acquisition of Brain Na Sensitivity Contributes to Salt-Induced Sympathoexcitation and Cardiac Dysfunction in Mice With Pressure Overload

Koji Ito, Yoshitaka Hirooka, Kenji Sunagawa

Abstract—In animal models of salt-sensitive hypertension, high salt augments sympathetic outflow via central mechanisms. It is not known, however, whether pressure overload affects salt sensitivity, thereby modifying central sympathetic outflow and cardiac function. We induced left ventricular hypertrophy with aortic banding in mice. Four weeks after aortic banding (AB-4), the left ventricle wall thickness was increased without changing the percentage fractional shortening. AB-4 mice were then fed either a high-salt (8%) diet or regular-salt diet for additional 4 weeks. Cardiac dysfunction, wall thickness, and 24-hour urinary catecholamine excretion were increased with high-salt diet compared with regular-salt diet. We then examined brain Na sensitivity. Intracerebroventricular infusion of high-Na (0.2 mol/L) artificial cerebrospinal fluid into AB-4 mice and mice Sham-4 increased urinary catecholamine excretion, arterial pressure, and heart rate more in AB-4 mice than in Sham-4 mice. Intracerebroventricular infusion of an epithelial Na channel blocker (benzamil) into mice with high-salt diet significantly decreased urinary catecholamine excretion and improved cardiac function. Infusion of either an angiotensin II type 1 receptor blocker or a Rho-kinase inhibitor also attenuated the salt-induced sympathetic hyperactivation and cardiac dysfunction in mice with high-salt diet. The levels of angiotensin II type 1 receptor and phosphorylated moesin, a substrate of Rho-kinase, were significantly greater in AB-4 mice than in Sham-4 mice. These results suggest that mice with pressure overload acquire brain Na sensitivity because of the activation of epithelial Na channel via Rho-kinase and angiotensin II, and this mechanism contributes to salt-induced sympathetic hyperactivation, further pressure overload, and cardiac dysfunction. (***Circ Res.* 2009;104:1004-1011.**)

Key Words: hypertension ■ heart failure ■ hypertrophy ■ sympathetic nervous system ■ brain ■ sodium chloride

As an environmental factor, high salt intake increases sympathetic activity in genetic models of hypertension.[1–3] In these salt-sensitive hypertensive rats, central mechanisms, such as enhanced Na sensitivity, as well as renal mechanisms contribute to high salt–induced sympathetic activation and arterial pressure elevation.[1–3] Enhanced central sympathetic outflow is also observed in animal models of heart failure,[4–7] and intracerebroventricular (ICV) infusion of an amiloride analog, benzamil, which inhibits the epithelium Na^+ channels (ENaCs), may reduce the enhanced sympathetic drive and improve cardiac function in rats with myocardial infarction.[4]

The effects of sustained cardiac pressure overload on cardiac function and/or cardiac muscles have been investigated using aortic banding models.[8,9] It is not known whether the sustained cardiac pressure overload without a genetic predisposition to salt sensitivity influences brain Na sensitivity. Furthermore, few studies have examined the relationship between central sympathetic outflow and cardiac function in animals with pressure overload. Therefore, the aim of the present study was to determine whether a sustained pressure overload produced in mice without a genetic predisposition to salt sensitivity induces brain Na sensitivity, thereby enhancing the central sympathetic outflow leading to cardiac dysfunction. For this purpose, we examined the effects of high salt intake on brain Na concentration, sympathetic activity, arterial pressure, and cardiac function in mice with pressure overload produced by aortic banding. To elucidate brain Na sensitivity, we infused high-Na artificial cerebrospinal fluid (aCSF) ICV in mice with or without pressure overload induced by aortic banding and evaluated sympathetic activity and arterial pressure. In addition, to determine whether brain Na sensitivity is acquired in this model, we examined the effects of the ENaC blocker benzamil[4,5] on high salt–induced activation of the sympathetic nervous system and arterial pressure elevation, because ENaCs on the blood side of the choroidal epithelium may have an important role in Na transport into the CSF, as well as Na^+-K^+ ATPase on the CSF side of choroidal epithelium.[3,10,11] In addition, to explore the mechanisms involved, we also evaluated the role of brain

Original received October 7, 2008; revision received March 5, 2009; accepted March 10, 2009.
From the Department of Cardiovascular Medicine, Kyushu University Graduate School of Medical Sciences, Fukuoka, Japan.
Correspondence to Yoshitaka Hirooka, MD, PhD, FAHA, Department of Cardiovascular Medicine, Kyushu University Graduate School of Medical Sciences, 3-1-1, Higashi-ku, Fukuoka 812-8582, Japan. E-mail hyoshi@cardiol.med.kyushu-u.ac.jp

Circulation Research **is available at http://circres.ahajournals.org** **DOI: 10.1161/CIRCRESAHA.108.188995**

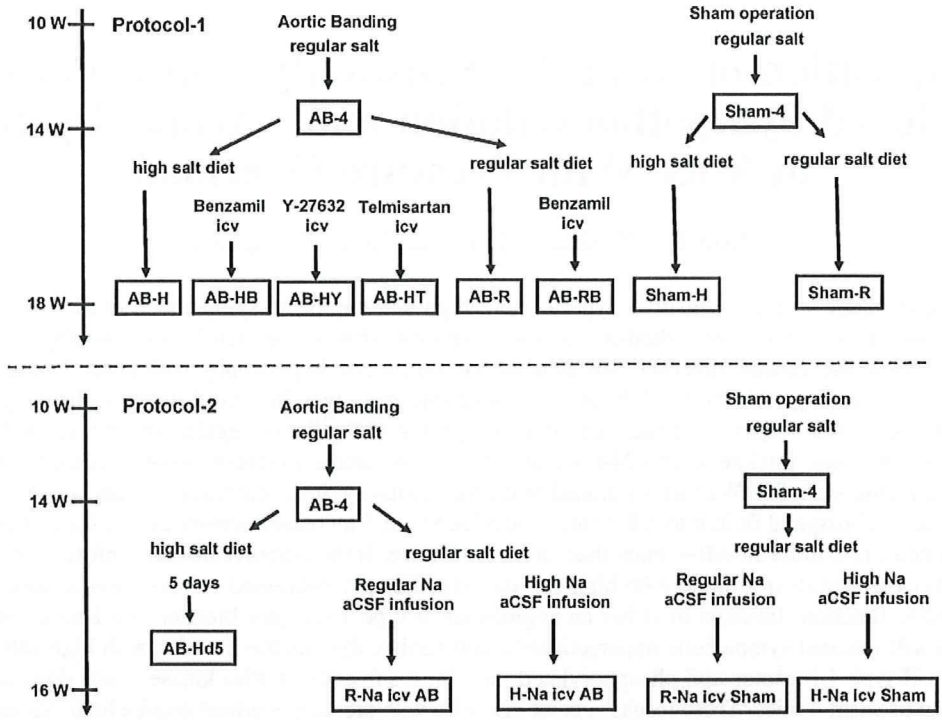

Figure 1. Experimental protocol and time line. W indicates weeks.

ENaCs in the enhanced sympathetic activity and cardiac dysfunction induced by high salt intake in mice with pressure overload and the relationship of brain ENaCs to the Rho/Rho-kinase pathway and the renin–angiotensin system (RAS) in the brain, because ENaCs in kidney are reported to be activated by the Rho/Rho-kinase pathway[12] and RAS.[13]

Materials and Methods

Animals

The study was reviewed and approved by the Committee on Ethics of Animal Experiments, Kyushu University Graduate School of Medical Sciences, and conducted according to the Guidelines for Animal Experiments of Kyushu University. Male Institute of Cancer Research (ICR) mice (10 weeks old; SLC, Fukuoka, Japan) were used.

Mouse Pressure Overload Model Preparation

The suprarenal abdominal aorta was banded in ICR mice (AB mice) to create the pressure overload model[14] or sham operation (Sham mice) as a control. We divided these mice into the groups represented in Figure 1. For details, see the online data supplement, available at http://circres.ahajournals.org.

Evaluation of Cardiac Function

Cardiac function was evaluated by echocardiography.[15,16] Serial M-mode echocardiography was performed under light sodium pentobarbital anesthesia with spontaneous respiration. Cardiac function was also evaluated by the left ventricular end-diastolic pressure (LVEDP). A conductance catheter (1.4 Fr; Miller Instruments) was inserted into the right carotid artery and advanced across the aortic valve into the left ventricle. See the online data supplement for details.

Measurement of Arterial Pressure and Heart Rate

Under sodium pentobarbital anesthesia and mechanical ventilation, a catheter was inserted into the right carotid artery and arterial pressure and heart rate were measured. In another protocol, we also measured arterial pressure and heart rate in awake AB mice fed a high-salt diet (AB-H) and AB mice fed with a regular salt diet (AB-R) using a radiotelemetry system implanted in the left carotid artery.[17] See the online data supplement for details.

Evaluation of Sympathetic Activity

Sympathetic activity was evaluated by measuring 24-hour urinary norepinephrine (U-NE) and urinary epinephrine (U-E) excretion using high-performance liquid chromatography.[15,18]

Evaluation of Na Sensitivity

We evaluated U-NE, U-E, arterial pressure, and heart rate responses to a high-salt diet or high-Na aCSF (0.2 mol/L, 1 μL/min for 10 minutes) ICV infusion in each group. In addition, we measured Na concentrations in the brain tissue (circumventricular tissues including the hypothalamus) of mice in each group. Furthermore, to examine the response of other central stimuli, we performed ICV infusion of angiotensin II (0.5 nmol/L, 1 μL/min for 5 minutes) and carbachol (0.1 mmol/L, 1 μL/min for 5 minutes). See the online data supplement for details.

Measurement of Organ Weight

After completion of the experiments, mice were killed with an overdose of sodium pentobarbital, and the heart and lungs were removed and weighed.

Measurement of Serum Parameters

We measured the serum concentrations of sodium, creatinine, and aldosterone in each group. See the online data supplement for details.

Evaluation of the Effects of Na Channel Blockade in the Brain

To assess the effects of Na channel blockade in the brain, benzamil, a specific ENaC blocker, was infused ICV (1 mg/ml, 0.11 μL/h for 28 days[14]). The U-NE and U-E excretion, arterial pressure, heart rate, and organ weight were measured, and echocardiography was per-

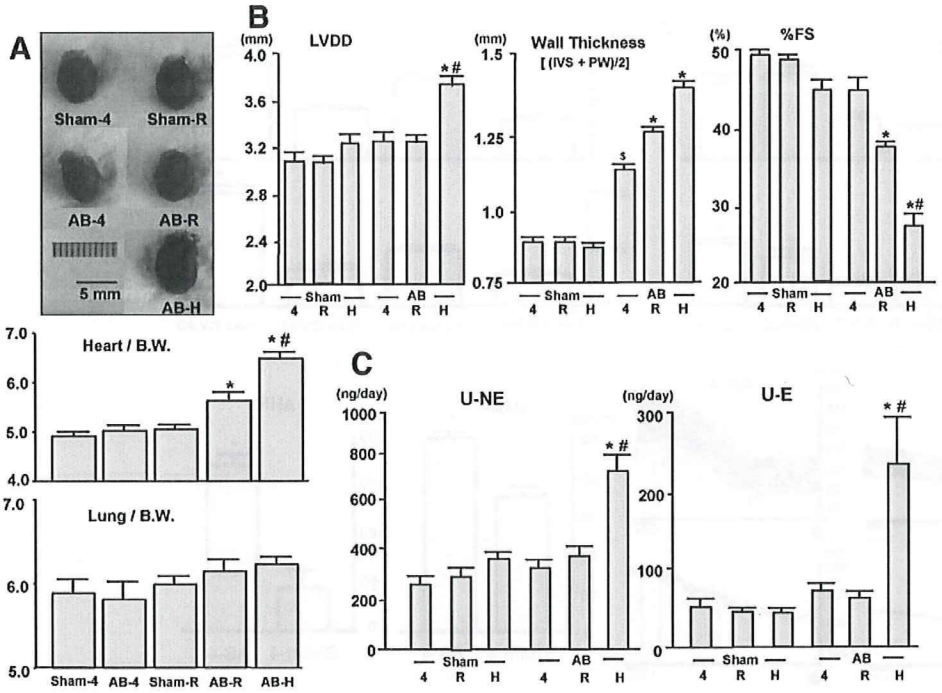

Figure 2. A, Example of the heart in each group and the relative heart and lung weight in each group. *$P<0.05$ vs Sham-4 and Sham-R, #$P<0.05$ vs AB-R (n=6 in each group). B, Cardiac function evaluation by echocardiography in each group. IVS, interventricular septum; PW, posterior wall. *$P<0.05$ vs Sham-R, #$P<0.05$ vs AB-R, \$$P<0.05$ vs Sham-4 (n=8 in each group). C, The 24-hour U-NE and U-E excretion in each group. *$P<0.05$ vs Sham-4 and Sham-R, #$P<0.05$ vs AB-R (n=10 in each group).

formed as described earlier. See the online data supplement for details.

Evaluation of the Effects of Rho-Kinase and Angiotensin Type 1 Receptor Blockade in the Brain

To assess the effects of Rho-kinase or angiotensin II type 1 receptor (AT_1R) blockade in the brain, Y-27632 (a specific Rho-kinase inhibitor[18]) or telmisartan (an AT_1R blocker) was infused ICV (Y-27632: 5 mmol/L, 0.11 μL/h for 28 days; telmisartan: 4 and 20 mmol /L, 0.11 μL/h for 28 days). The U-NE and U-E excretion, arterial pressure, heart rate, and organ weight were measured, and echocardiography was performed as described earlier. See the online data supplement for details.

Evaluation of AT_1R Expression and Rho-Kinase Activity

To assess AT_1R expression levels and Rho-kinase activity, we performed a Western blot analysis for AT_1R (1:1000, Santa Cruz Biotechnology, Santa Cruz, Calif) and phosphorylated-moesin, a substrate of Rho-kinase[19] (p-moesin, 1:1000, Santa Cruz Biotechnology) in the circumventricular tissues, including the hypothalamus and brain stem tissues, of Sham-4 mice and AB-4 mice. See the online data supplement for details.

Statistical Analysis

All values are expressed as means±SE. ANOVA was used to compare U-NE and U-E excretion, organ weight, left ventricular end-diastolic diameter (LVDD), left ventricular wall thickness (LVWT), percentage fractional shortening (%FS), and arterial pressure measured by telemetry between groups. An unpaired *t* test was used to compare changes in arterial pressure and heart rate after high-Na ICV infusion, as well as protein levels, between Sham mice and AB mice. Differences were considered to be significant when $P<0.05$.

Results

Characteristics of the Pressure Overload Model

Relative heart weight (heart weight/body weight) was not increased in AB-4 mice compared with Sham-4 mice (Figure 2A). AB-R mice, however, had a significantly higher relative heart weight than Sham-R mice and a significantly lower relative heart weight than AB-H mice. Relative lung weight (lung weight/body weight) did not differ between groups (Figure 2A). Body weight of AB mice was significantly lower than that of Sham mice (body weight: Sham-4, 44.7±1.4 g; AB-4, 45.3±1.1 g; Sham-R, 47.8±0.5 g; AB-R, 42.5±0.6 g; AB-H 40.6±0.9 g, n=6 for each); however, the absolute heart weight in AB-H was significantly greater than that in AB-R or Sham-R mice (heart weight: AB-H 0.26±0.01 g; Sham-R 0.24±0.01 g; AB-R 0.24±0.01 g; n=6 for each).

Echocardiography revealed the following characteristics: LVWT was greater in AB-4 mice than in Sham-4 mice, but %FS did not differ between the groups (Figure 2B). After an additional 4 weeks, cardiac function declined in AB-R mice compared with Sham-R mice and declined significantly more in AB-H mice compared with AB-R mice. LVDD was also higher in AB-H mice than in AB-R mice (Figure 2B).

Sympathetic activity was not significantly different among the AB-4 mice, AB-R mice, Sham-4 mice, and Sham-R mice. U-NE and U-E excretion was significantly higher, however, in AB-H mice compared with the other groups (Figure 2C).

LVEDP was significantly higher in AB-4 mice than in Sham-4 mice. In addition, LVEDP in AB-H mice further increased compared with Sham-R or AB-R mice (Table I in the online data supplement).

Arterial Pressure Monitoring

Measurement Under Anesthesia

Mean arterial pressure and heart rate were significantly higher in AB-4 mice compared with Sham-4 mice. In AB-R and AB-H mice, arterial pressure was reduced to levels similar to that in the Sham-R mice. Heart rate was significantly higher in AB-4, AB-R, and AB-H mice than in Sham-4

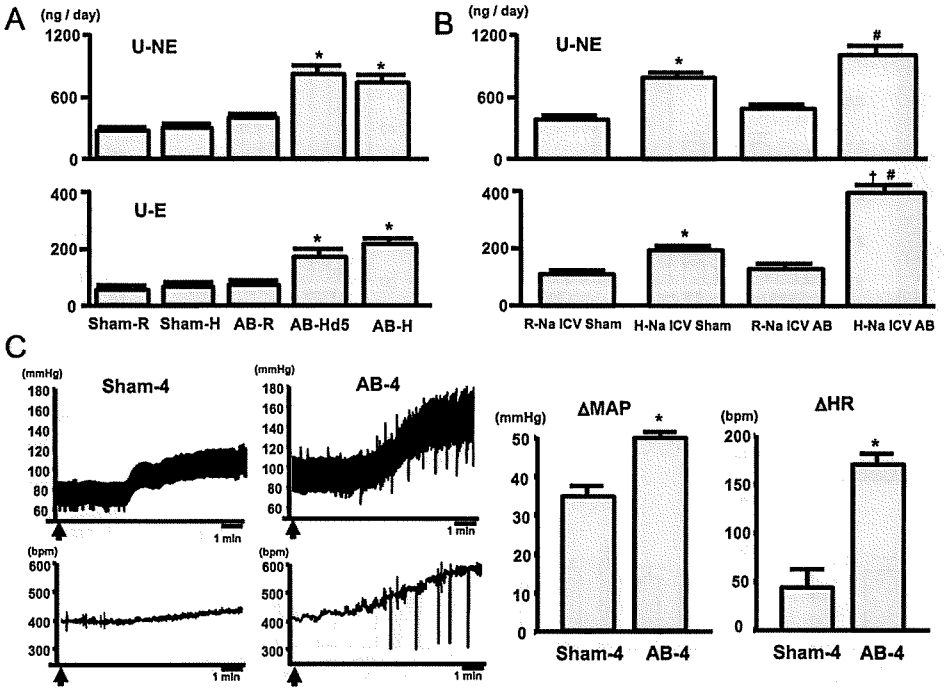

Figure 3. A, The 24-hour U-NE and U-E excretion in each group (response of sympathetic activity to high-salt diets). *$P<0.05$ vs Sham-R, Sham-H, and AB-R (n=10 in each group). B, The 24-hour U-NE and U-E excretion in each group (response of sympathetic activity to high-Na aCSF ICV infusion). *$P<0.05$ vs ICV R-Na Sham, #$P<0.05$ vs ICV R-Na AB, †$P<0.05$ vs high-Na ICV Sham (n=5 in each group). C, Response of arterial pressure and heart rate to ICV high-Na aCSF infusion. Left, Representative recordings from Sham-4 and AB-4 showing arterial pressure and heart rate response to ICV high-Na aCSF infusion. Right, Group data of mean arterial pressure and heart rate response to ICV high-Na aCSF infusion in Sham-4 and AB-4. *$P<0.05$ vs Sham (n=3 in each group).

or Sham-R mice. There were no significant differences in arterial pressure and heart rate between the groups of Sham mice (Online Table II).

Measurement in Awake Mice Using Radio-Telemetry System

In AB-4 mice (AB day 28), mean arterial pressure and heart rate were significantly higher than that in the mice before aortic banding. Furthermore, high salt intake (AB-H mice) dramatically increased mean arterial pressure to 171±5 mm Hg by day 35 after aortic banding (1 week after the starting high salt intake). The general conditions deteriorated in all AB-H mice, however, likely because of severe lung congestion (lung/body weight ratio, 7.0±0.1). In AB-R mice, mean arterial pressure increased mildly, and the highest mean arterial pressure value was 145±5 mm Hg on day 38 after aortic banding and thereafter gradually decreased to 124±7 mm Hg on day 56 after aortic banding (n=3 for each; see the online data supplement for details).

Salt Sensitivity in Sham Mice and AB Mice

High salt intake did not increase U-NE or U-E excretion in Sham mice (Figure 3A). In AB mice, however, high salt intake significantly increased U-NE and U-E excretion. Furthermore, U-NE excretion in AB mice began to increase within 5 days (AB-Hd5 mice) of beginning the high-salt diet (Figure 3A), although cardiac function was preserved (%FS 43±1%; n=5). ICV infusion of regular-Na aCSF did not significantly increase U-NE or U-E excretion in Sham mice or AB mice (Figure 3B). ICV infusion of high-Na aCSF significantly increased U-NE and U-E excretion in both Sham mice and AB mice. The increase in U-NE excretion in AB mice, however, tended to be greater than that in Sham mice ($P=0.1$), and the increase in U-E excretion was significantly greater in AB mice than in Sham mice (Figure 3B).

In the acute experiments, high-Na aCSF ICV infusion increased arterial pressure and heart rate in both Sham-4 mice and AB-4 mice, but the degree of these changes was significantly greater in AB-4 mice (Figure 3C). The pressor response to angiotensin II ICV infusion was greater in AB-4 mice than Sham-4 mice (ΔMAP 8.6±1.2 mm Hg in Sham-4, 22.3±3.4 mm Hg in AB-4 mice, n=4 for each), however, the pressor response to carbachol ICV infusion did not differ between groups (ΔMAP: 9.5±1.8 mm Hg in Sham-4, 13.7±1.5 mm Hg in AB-4 mice; n=4 for each).

Na concentration in the brain tissues (circumventricular tissues including hypothalamus) was higher in AB-H mice than in the other groups (AB-H, 116±2 ppm; AB-R, 102±4 ppm; Sham-R, 104±2 ppm; Sham-H, 104±2 ppm; n=5 for each; $P<0.05$).

Effects of High-Na aCSF ICV Infusion on Cardiac Function

In AB mice, high-Na aCSF ICV infusion significantly increased LVDD (3.4±0.4 mm) and decreased %FS (32±1%) compared with regular-Na aCSF ICV infusion (LVDD, 3.2±0.5 mm; %FS, 41±1%; n=5 for each; $P<0.05$). Arterial pressure did not differ between AB mice with high-Na aCSF and regular-Na aCSF (94±3 mm Hg in high-Na aCSF,

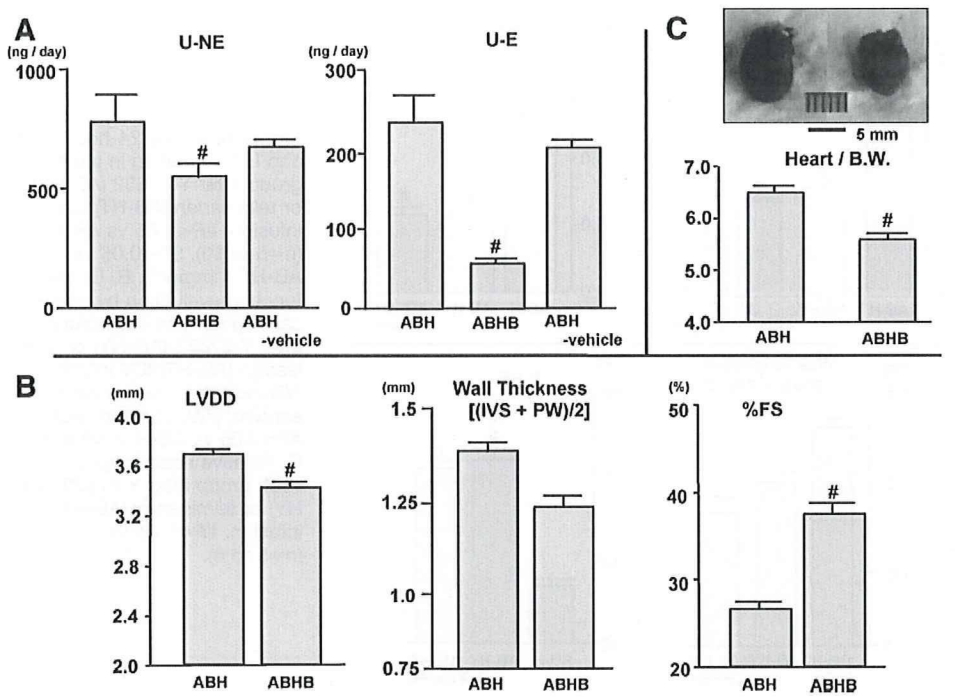

Figure 4. A, The 24-hour U-NE and U-E excretion in each group after ICV benzamil (AB-HB) infusion. #$P<0.05$ vs AB-H (n=5 to 10). B, Cardiac function evaluation by echocardiography in each group. IVS indicates interventricular septum; PW, posterior wall. #$P<0.05$ vs AB-H (n=8 in each group). C, Relative heart weight in each group. #$P<0.05$ vs AB-H (n=6 in each group).

101±5 mm Hg in regular-Na aCSF; n=4 for each). In Sham mice, high-Na aCSF ICV infusion had no significant effects on cardiac function compared with regular-Na aCSF ICV infusion (LVDD, 3.1±0.2 mm in high-Na aCSF versus 3.1±0.3 mm in regular-Na aCSF; %FS, 46±2% in high-Na aCSF versus 48±3% in regular-Na aCSF; n=5 for each).

Effects of ENaC Blocker ICV Infusion on Cardiac Function

In comparison with AB-H mice, ICV infusion of the ENaC blocker benzamil (AB-HB mice) significantly decreased U-NE and U-E excretion (Figure 4A). Cardiac function (LVDD and %FS) significantly improved in AB-HB mice compared with AB-H mice (Figure 4B). Relative heart weight decreased in AB-HB mice compared with AB-H mice (Figure 4C). Arterial pressure was significantly higher and heart rate was lower in AB-HB mice than in AB-H mice (Online Table II). ICV infusion of benzamil did not affect these measures in AB-R mice, and ICV infusion of vehicle in AB-H mice also did not significantly decrease U-NE and U-E excretion (data not shown).

Rho-Kinase Activity and AT_1R Expression in the Brain

The amount of AT_1R and the expression of p-moesin, a substrate of Rho-kinase, in the brain stem and circumventricular tissue were significantly higher in AB-4 mice than in Sham-4 mice (Figure 5).

Effects of ICV Infusion of Rho-Kinase Inhibitor and AT_1R Blocker on Cardiac Function

In comparison with AB-H mice, ICV infusion of the Rho-kinase inhibitor Y-27632 (AB-HY mice) or AT_1R blocker telmisartan (AB-HT mice) induced a significant decrease in U-NE and U-E excretion (Figure 6A). In AB-HT mice, U-NE and U-E decreased in a dose-related manner. Cardiac function was also significantly improved in AB-HY mice or AB-HT mice compared with AB-H mice (Figure 6B). Relative heart weight was decreased in AB-HY mice or AB-HT mice compared with AB-H mice (Figure 6C). Heart rate was significantly decreased in AB-HY mice or AB-HT mice compared with AB-H mice (Online Table II). Infusion of vehicle (aCSF or DMSO) did not have these effects.

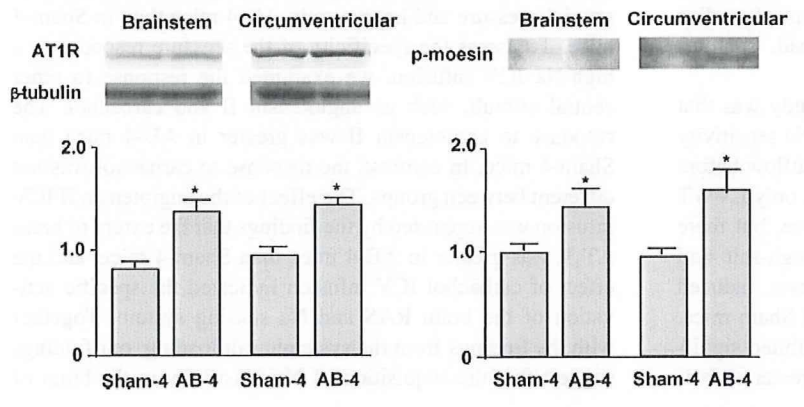

Figure 5. Left, Representative Western blots demonstrating the expression of AT_1R in the brain (circumventricular tissues including hypothalamus and brain stem tissues) of Sham-4 or AB-4. The graph shows the means for the quantification of 4 separate experiments. Data are expressed as the relative ratio to β-tubulin expression (n=4 in each group). *$P<0.05$ vs Sham-4. Right, Representative Western blot demonstrating the expression of p-moesin, a substrate of Rho-kinase in the brain (circumventricular tissues including hypothalamus and brain stem tissues) of Sham-4 or AB-4. The graph shows the means for the quantification of 3 separate experiments. Data are expressed as the relative ratio to Sham-4, which was assigned a value of 1 (n=3 in each group). *$P<0.05$ vs Sham.

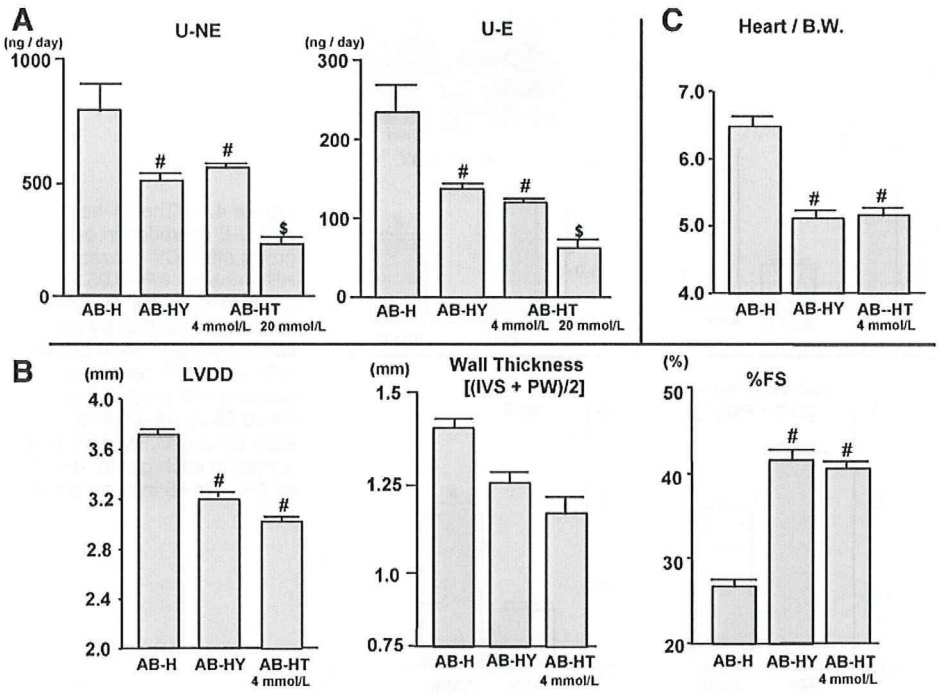

Figure 6. A, The 24-hour U-NE and U-E excretion in each group after Y-27632 (AB-HY) or telmisartan (AB-HT) ICV infusion. #$P<0.05$ vs AB-H (n=5 to 10), \$$P<0.05$ vs AB-HT 4 mmol/L. B, Cardiac function evaluation by echocardiography in each group after Y-27632 (AB-HY) or telmisartan (AB-HT) ICV infusion. IVS indicates interventricular septum; PW, posterior wall. #$P<0.05$ vs AB-H (n=5 to 8). C, Relative heart weight in each group after Y-27632 (AB-HY) or telmisartan (AB-HT) ICV infusion. #$P<0.05$ vs AB-H (n=5 to 6).

Serum Parameters

Serum Na concentration did not differ between groups (Sham-4, 151±2 mEq/L; AB-4, 151±1 mEq/L; AB-R, 150±1 mEq/L; AB-H, 152±1 mEq/L). Serum creatinine concentration, as a marker of renal function, also did not differ between groups (Sham-4, 0.11±0.01 mg/dL; AB-4, 0.09±0.01 mg/dL; AB-R, 0.12±0.01 mg/dL; AB-H, 0.11±0.01 mg/dL). Serum aldosterone levels were not different between Sham-4 and AB-4 mice and were significantly lower in AB-H mice than in AB-4 mice, AB-R mice, and Sham-4 mice (Sham-4, 120±11 pg/dL; AB-4, 145±28 pg/dL; AB-R, 163±17 pg/dL; AB-H, 54±6 pg/dL; n=6 to 7; $P<0.05$).

Discussion

The major findings of the present study were that mice with pressure overload produced by aortic banding acquired brain Na sensitivity via the activation of brain ENaCs through stimulation of the Rho/Rho-kinase pathway and RAS. Because of the acquired brain Na sensitivity, high salt intake led to sympathetic activation, which led to the deterioration of cardiac function. These findings are novel and suggest new targets for studies of the prevention and treatment of cardiac deterioration in patients with pressure overload, such as hypertensive heart disease.

The most important finding of the present study was that the mice with pressure overload acquired brain Na sensitivity and a high-salt diet increased the sympathetic outflow before cardiac dysfunction was detected. In AB-4 mice, only LVWT tended to increase compared to the Sham-4 mice, but there was no effect on cardiac function. Both a high-salt and regular-salt diet for an additional 4 weeks, however, induced cardiac dysfunction in AB mice compared with Sham mice. Furthermore, AB mice on the high-salt diet exhibited significantly more severe cardiac dysfunction and greater activation of the sympathetic system than AB mice on the regular-salt diet. This high-salt induced enhanced sympathetic drive was obvious before cardiac function was impaired. In Sham mice, a high salt intake did not increase U-NE and U-E excretion and had no effect on cardiac function. These results strongly suggest that the mice with pressure overload acquired the salt sensitivity before cardiac function began to deteriorate and that a high salt intake augmented cardiac dysfunction by inducing sympathetic activation.

To clarify the contribution of central mechanisms to the acquisition of salt sensitivity in mice with pressure overload, we examined the effects of high-Na in the CSF on sympathetic activity and arterial pressure after ICV infusion of high-Na or regular-Na aCSF. Compared with ICV infusion of regular-Na aCSF, high-Na aCSF induced significant increases in U-NE and U-E excretion in both groups of mice. The increased U-NE excretion in AB mice, however, tended to be greater than that in Sham mice ($P=0.1$), and the increase in U-E excretion was significantly greater in AB mice than in Sham mice. Furthermore, ICV infusion of high-Na aCSF induced significantly greater increases in arterial pressure and heart rate in AB-4 mice than in Sham-4 mice. To assess the specificity of the pressure response to a high-Na ICV infusion, we examined the response to other central stimuli, such as angiotensin II and carbachol. The response to angiotensin II was greater in AB-4 mice than Sham-4 mice. In contrast, the response to carbachol was not different between groups. The effect of the angiotensin II ICV infusion was supported by the findings that the extent of brain AT_1R was greater in AB-4 mice than Sham-4 mice, and the effect of carbachol ICV infusion indicated the specific activation of the brain RAS and Na sensing system. Together with the findings from the systemic salt loading, our findings suggest that the acquisition of Na sensitivity in the brain of

mice with pressure overload results from two different mechanisms: (1) the enhancement of Na uptake into the brain and (2) the increase in responsiveness to Na within the brain.

Another important finding of the present study was the high-Na aCSF-induced activation of the sympathetic system, which further deteriorates cardiac function in mice with pressure overload. There are some reports that enhanced sympathetic drive plays an important role in the progression of heart failure.[20,21] In the present study, in comparison with ICV infusion of regular-Na aCSF, high-Na aCSF induced a significant decline in cardiac function. To evaluate the possibility that the increase in the afterload induced by increased arterial pressure affected cardiac function, we measured arterial pressure 2 weeks after ICV infusion of high-Na aCSF and confirmed that arterial pressure did not significantly increase compared with regular-Na ICV infusion. These results suggest that high-Na aCSF-induced sympathetic hyperactivation may lead to cardiac dysfunction in mice with pressure overload and the deterioration of cardiac function may not be attributable to the increase in the afterload induced by the arterial pressure elevation. However, high-salt loading caused further decreases in cardiac function in AB mice, indicating that high-salt loading may induce further decrease in cardiac function both by sympathetic activation and an increase in arterial pressure in AB mice.

Arterial pressure in AB-4 mice was significantly higher than that in Sham-4 mice; and arterial pressure in AB-H 1-week mice, which were loaded with a high-salt diet for 1 week, was further increased compared with that in AB-4 mice. Arterial pressure in AB-R mice and AB-H mice decreased to levels similar or lower than that in Sham mice within 8 weeks. This may relate to cardiac dysfunction. In fact, the LVEDP in AB-H mice was significantly greater than that in AB-R or Sham-R mice and the LV %FS in AB-H mice was significantly smaller than that in AB-R or Sham-R mice. To validate the arterial pressure measurements, we measured arterial pressure and heart rate using a radio-telemetry system with mice in the awake state. At day 28 after aortic banding (AB-4 mice), arterial pressure was significantly higher than that before aortic banding. Thereafter, in AB-H mice, arterial pressure was significantly further increased at day 35 (1 week after the starting high-salt diet), but the general health of the mice deteriorated, likely because of severe lung congestion, which was supported by the high lung/body weight ratio. In AB-R mice, arterial pressure peaked at around day 40 and then gradually decreased. Implantation of the telemetry catheter in the carotid artery might further augment the pressure overload and induce severe lung congestion in AB-H mice. Therefore, we examined the arterial pressure under anesthesia in acute experiments. The findings indicate that aortic banding causes a pressure overload for LV and high-salt loading superimposed on aortic banding further augments the pressure overload.

To explore the mechanisms of the acquisition of brain Na sensitivity, we examined the effects of an ENaC blocker, benzamil. Brain ENaCs are involved in the high salt–induced increase in central sympathetic outflow in salt-sensitive hypertensive rats.[1,3] In the present study, brain ENaC blockade by benzamil attenuated the high salt–induced activation of the sympathetic nervous system and the deterioration of cardiac function. Furthermore, we examined the brain Na concentrations in each group. We were unable to measure Na concentrations in the CSF in the present study, because in mice it is difficult to obtain the volume of CSF required to measure Na concentration. Therefore, we measured the Na concentrations in the brain tissues and confirmed that AB-H mice had higher Na concentrations than the other groups. These findings support our hypothesis that the pressure overload activates brain ENaCs and augments Na transport from plasma to the CSF, resulting in sympathoexcitation. However, we did not examine the effects of brain ENaCs on Na transport directly and ENaCs have both epithelial and neural components.[11] Therefore, it is possible that the benzamil may affect ENaCs on neural components and cause sympathoinhibitory effects. The role of ENaCs on neural components in sympathetic modulation remains unclear. A similar dose of benzamil was used as specific ENaC blocker in previous studies,[4] and the estimated benzamil concentration in the CSF in the present study was considered to be specific for ENaCs (<100 nmol/L).[22–24] Therefore, the dose of benzamil used in the present study was adequate for use as a specific ENaC blocker. Further studies are required to measure ENaC activity directly. Although some studies have demonstrated that salt intake induces sympathoexcitation via central mechanisms[1–3] and the effects of brain ENaCs on cardiac function,[4] these previous studies used genetic models of salt-sensitive hypertension or heart failure induced by myocardial infarction, whereas we used the pressure overload produced by aortic banding model in mice without a genetic background of salt sensitivity.

Finally, we focused on Rho-kinase and angiotensin II as the mechanisms involved in brain ENaC activation in the mice with pressure overload, because ENaCs in kidney are reported to be activated by Rho-kinase[12] and angiotensin II.[13] In addition, we recently reported that Rho-kinase[16,25–27] and angiotensin II[28] in the brain contribute to cardiovascular regulation via the sympathetic nervous system. In the present study, we confirmed that compared to Sham-4 mice, the brains of AB-4 mice had higher levels of AT_1R and higher Rho-kinase activity, and blockade of either AT_1R or Rho-kinase attenuates high salt–induced sympathetic activation and cardiac dysfunction. These findings suggest that enhanced brain Na sensitivity results from the activation of brain ENaCs via the Rho/Rho-kinase pathway and RAS in mice with pressure overload. However, ENaCs may be upstream of RAS in brain.[29] In the present study, we did not address this issue. Further studies are needed to clarify the relationship between RAS and ENaCs in brain. It is possible that renal blood flow is reduced in mice with suprarenal abdominal aortic banding, resulting in renal dysfunction[30] concomitant with activation of the systemic RAS.[31] It is unlikely that this occurred in the present study because we confirmed that serum creatinine and aldosterone levels were not significantly different between groups and the mean arterial pressure in the AB-4 mice measured from the right femoral artery was above 90 mm Hg, suggesting that the aortic banding procedure did not significantly reduce renal blood flow and impair renal function. Previous studies

demonstrated that excess stimulation of cardiopulmonary and arterial baroreceptors impair baroreflex function[32,33] and RAS[32] or Rho-kinase[33] in the brain might contribute to the impaired baroreflex function. In the present study, we demonstrated that arterial pressure measured from the carotid artery and LVEDP were significantly greater in AB-4 mice than in Sham-4 mice. The excess stimulation of cardiopulmonary and arterial baroreceptor may contribute to the activation of the Rho/Rho-kinase pathway and RAS in the brains of the mice with pressure overload, even before high-salt loading.

In conclusion, the present findings strongly suggest that mice with pressure overload acquire brain Na sensitivity because of the activation of brain ENaCs via the Rho/Rho-kinase pathway and RAS. The acquired brain Na sensitivity contributes to high salt–induced sympathetic activation, leading to deteriorating cardiac function in mice with pressure overload.

Sources of Funding

This work was supported by Grants-in-Aid for Scientific Research from the Japan Society for the Promotion of Science (B19390231 and 19890148) and the Mitsubishi Pharma Research Foundation.

Disclosures

None.

References

1. Nishimura M, Ohtsuka K, Nanbu A, Takahashi H, Yoshimura M. Benzamil blockade of brain Na^+ channels averts Na^+-induced hypertension in rats. *Am J Physiol*. 1998;274:R635–R644.
2. Fujita M, Ando K, Nagae A, Fujita T. Sympathoexcitation by oxidative stress in the brain mediates arterial pressure elevation in salt-sensitive hypertension. *Hypertension*. 2007;50:360–367.
3. Huang BS, Amin MS, Leenen FHH. The central role of the brain in salt-sensitive hypertension. *Curr Opin Cardiol*. 2006;21:295–304.
4. Huang BS, Leenen FHH. Blockade of brain mineralcorticoid receptors or Na^+ channels prevents sympathetic hyperactivity and improve cardiac function in rats post-MI. *Am J Physiol*. 2005;288:H2491–H2497.
5. Leenen FHH. Brain mechanisms contributing to sympathetic hyperactivity and heart failure. *Circ Res*. 2007;101:221–223.
6. Mark AL. Sympathetic dysregulation in heart failure: mechanisms and therapy. *Clin Cardiol*. 1995;18:I3–I8.
7. Zucker IH. Novel mechanisms of sympathetic regulation in chronic heart failure. *Hypertension*. 2006;48:1005–1011.
8. Takimoto E, Champion HC, Li M, Belardi D, Ren S, Rodriguez ER, Bedja D, Gabrielson KL, Wang Y, Kass DA. Chronic inhibition of cyclic phosphodiesterase 5A prevents and reverse cardiac hypertrophy. *Nat Med*. 2005;11:214–222.
9. Klotz S, Hay I, Zhang G, Maurer M, Wang J, Burkhoff D. Development of heart failure in chronic hypertensive Dahl rats focus on heart failure with preserved ejection fraction. *Hypertension*. 2006;47:901–911.
10. Vigne P, Champigny G, Marsaut R, Barbry P, Frelin C, Lazdunski M. A new type of amiloride-sensitive cation channel in endothelial cells of brain microvessels. *J Biol Chem*. 1989;264:7663–7668.
11. Amin MS, Wang HW, Reza E, Whitman SC, Tuana BS, Leenen FHH. Distribution of epithelial sodium channels and mineralocorticoid receptors in cardiovascular regulatory centers in rat brain. *Am J Physiol*. 2005;289:R1787–R1797.
12. Pochynyuk O, Medina J, Gamper N, Genth H, Stockand JD, Staruschenko A. Rapid translocation and insertion of the epithelial Na^+ channel in response to RhoA signaling. *J Biol Chem*. 2006;281:26520–26527.
13. Peti-Peterdi J, Warnock DG, Bell PD. Angiotensin II directly stimulates ENaC activity in the cortical collecting duct via AT1 receptors. *J Am Soc Nephrol*. 2002;13:1131–1135.
14. Harada K, Komuro I, Shiojima I, Hayashi D, Kudoh S, Mizuno T, Kijima K, Matsubara H, Sugaya T, Murakami K, Yazaki Y. Pressure overload induces cardiac hypertrophy in angiotensin II type II 1A receptor knockout mice. *Circulation*. 1998;97:1952–1959.
15. Sakai K, Hirooka Y, Shigematsu H, Kishi T, Ito K, Shimokawa H, Takeshita A, Sunagawa K. Overexpression of eNOS in brain stem reduces enhanced sympathetic drive in mice with myocardial infarction. *Am J Physiol Heart Circ Physiol*. 2005;289:H2159–H2166.
16. Ito K, Kimura Y, Hirooka Y, Sagara Y, Sunagawa K. Activation of Rho-kinase in the brainstem enhances sympathetic drive in mice with heart failure. *Auton Neurosci*. 2008;142:77–81.
17. Wirth A, Benyó Z, Lukasova M, Leutgeb B, Wettschureck N, Gorbey S, Örsy P, Horváth B, Maser-Gluth C, Greiner E, Lemmer B, Schütz G, Gutkind S, Offermanns S. G_{12}-G_{13}-LARG-mediated signaling in vascular smooth muscle is required for salt-induced hypertension. *Nat Med*. 2008;14:64–68.
18. Uehata M, Ishizaki T, Satoh H, Ono T, Kawahara T, Morishita T, Tamakawa H, Yamagami K, Inui J, Maekawa M, Narumiya S. Calcium sensitization of smooth muscle mediated by a Rho-associated protein kinase in hypertension. *Nature*. 1997;389:990–994.
19. Matsui T, Maeda M, Doi Y, Yonemura S, Amano M, Kaibuchi K, Tsukita S. Rho-kinase phosphorylate COOH-terminal threonines of ezrin/radixin/moesin (ERM) proteins and regulates their head-to-tail association. *J Cell Biol*. 1998;140:647–657.
20. Cohn JN, Levine TB, Olivari MT, Garberg V, Lura D, Francis GS, Simon AB, Rector T. Plasma norepinephrine as a guide to prognosis in patients with chronic congestive heart failure. *N Engl J Med*. 1984;311:819–823.
21. Rector TS, Olivari MT, Levine TB, Francis GS, Cohn JN. Predicting survival for an individual with congestive heart failure using the plasma norepinephrine concentration. *Am Heart J*. 1987;114:148–152.
22. Teiwes J, Toto RD. Epithelial sodium channel inhibition in cardiovascular disease. *Am J Hypertens*. 2007;20:109–117.
23. Hirsh AJ, Sabater JR, Zamurs A, Smith RT, Paradiso AM, Hopkins S, Abraham WM, Boucher RC. Evaluation of second generation amiloride analogs as therapy for cystic fibrosis lung disease. *J Pharmacol Exp Ther*. 2004;311:929–938.
24. Rudick RA, Zirretta DK, Herndon RM. Clearance of albumin from mouse subarachnoid space: a measure of CSF bulk flow. *J Neurosci Methods*. 1982;6:253–259.
25. Ito K, Hirooka Y, Sakai K, Kishi T, Kaibuchi K, Shimokawa H, Takeshita A. Rho/Rho-kinase pathway in brain stem contributes to blood pressure regulation via sympathetic nervous system: possible involvement in neural mechanisms of hypertension. *Circ Res*. 2003;92:1337–1343.
26. Ito K, Hirooka Y, Kishi T, Kimura Y, Kaibuchi K, Shimokawa H, Takeshita A. Rho/Rho-kinase pathway in the brainstem contributes to hypertension caused by chronic nitric oxide synthase inhibition. *Hypertension*. 2004;43:156–162.
27. Ito K, Hirooka Y, Kimura Y, Sagara Y, Sunagawa K. Ovariectomy augments hypertension through Rho-kinase activation in the brain stem in female spontaneously hypertensive rats. *Hypertension*. 2006;48:651–657.
28. Sagara Y, Hirooka Y, Nozoe M, Ito K, Kimura Y, Sunagawa K. Pressor response induced by central angiotensin II is mediated by activation of Rho/Rho-kinase pathway via AT_1 receptors. *J Hypertens*. 2007;25:399–406.
29. Huang BS, Cheung WJ, Wang Hao, Tan J, White RA, Leenen FHH. Activation of brain renin-angiotensin-aldosterone system by central sodium in Wister rats. *Am J Physiol*. 2006;291:H1109–H1117.
30. Akers WS, Cross A, Speth R, Dwoskin LP, Cassis LA. Renin-angiotensin system andsympathetic nervous system in cardiac pressure-overload hypertrophy. *Am J Physiol*. 2000;279:H2797–H2806.
31. Héliés-Toussaint C, Moinard C, Rasmusen C, Tabbi-Anneni I, Cynober L, Gryngerg A. Aortic banding in rats as a model to investigate malnutrition associated with heart failure. *Am J Physiol*. 2005;288:R1325–R1331.
32. Wang WZ, Gao L, Pan YX, Zucker IH, Wang W. AT1 receptor in the nucleus tractus solitarii mediate the interaction between the baroreflex and the cardiac sympathetic afferent reflex in anesthetized rats. *Am J Physiol*. 2007;292:R1137–R1145.
33. Ito K, Hirooka Y, Sagara Y, Kimura Y, Kaibuchi K, Shimokawa H, Takeshita A, Sunagawa K. Inhibition of Rho-kinase in the brainstem augments baroreflex control of heart rate in rats. *Hypertension*. 2004;44:478–483.

Inhibition of Tumor Necrosis Factor-α–Induced Interleukin-6 Expression by Telmisartan Through Cross-Talk of Peroxisome Proliferator-Activated Receptor-γ With Nuclear Factor κB and CCAAT/Enhancer-Binding Protein-β

Qingping Tian, Ryohei Miyazaki, Toshihiro Ichiki, Ikuyo Imayama, Keita Inanaga, Hideki Ohtsubo, Kotaro Yano, Kotaro Takeda, Kenji Sunagawa

Abstract—Telmisartan, an angiotensin II type 1 receptor antagonist, was reported to be a partial agonist of peroxisome proliferator-activated receptor-γ. Although peroxisome proliferator-activated receptor-γ activators have been shown to have an anti-inflammatory effect, such as inhibition of cytokine production, it has not been determined whether telmisartan has such effects. We examined whether telmisartan inhibits expression of interleukin-6 (IL-6), a proinflammatory cytokine, in vascular smooth muscle cells. Telmisartan, but not valsartan, attenuated IL-6 mRNA expression induced by tumor necrosis factor-α (TNF-α). Telmisartan decreased TNF-α–induced IL-6 mRNA and protein expression in a dose-dependent manner. Because suppression of IL-6 mRNA expression was prevented by pretreatment with GW9662, a specific peroxisome proliferator-activated receptor-γ antagonist, peroxisome proliferator-activated receptor-γ may be involved in the process. Telmisartan suppressed IL-6 gene promoter activity induced by TNF-α. Deletion analysis suggested that the DNA segment between −150 bp and −27 bp of the IL-6 gene promoter that contains nuclear factor κB and CCAAT/enhancer-binding protein-β sites was responsible for telmisartan suppression. Telmisartan attenuated TNF-α–induced nuclear factor κB– and CCAAT/enhancer-binding protein-β–dependent gene transcription and DNA binding. Telmisartan also attenuated serum IL-6 level in TNF-α–infused mice and IL-6 production from rat aorta stimulated with TNF-α ex vivo. These data suggest that telmisartan may attenuate inflammatory process induced by TNF-α in addition to the blockade of angiotensin II type 1 receptor. Because both TNF-α and angiotensin II play important roles in atherogenesis through enhancement of vascular inflammation, telmisartan may be beneficial for treatment of not only hypertension but also vascular inflammatory change. (***Hypertension.* 2009;53: 798-804.)**

Key Words: interleukin-6 ■ TNF-α ■ PPARγ ■ NF-κB ■ C/EBPβ

Angiotensin II (Ang II) is a main final effecter molecule of the renin–angiotensin system. Physiologically, Ang II plays an important role in the regulation of blood pressure, fluid volume, and electrolyte balance.[1] However, Ang II is also involved in the pathological processes, such as cardiovascular diseases, renal insufficiency, and metabolic disorders.[2] Indeed, inhibition of the renin–angiotensin system by Ang II type 1 receptor (AT1R) antagonists has been proven beneficial for treatment of heart failure,[3] chronic kidney diseases,[4] and myocardial infarction.[5] AT1R antagonists also showed favorable effects on prevention of new onset of diabetes mellitus and atrial fibrillation.[6,7]

Telmisartan, one of the AT1R antagonists, was reported to be a partial agonist of peroxisome proliferator-activated receptor-γ (PPARγ).[8,9] PPARγ is a nuclear receptor transcription factor,[10] and the target genes of PPARγ are involved in the regulation of lipid and glucose metabolism and adipocyte differentiation. In addition, it is reported that thiazolidinediones (TZDs), synthetic PPARγ ligands, have an anti-inflammatory effect and inhibit atherogenesis.[11] The anti-inflammatory effect of TZDs involves inhibition of the function of nuclear factor κB (NF-κB), which plays an important role in the expression of many genes mediating an inflammatory process.[12]

Interleukin-6 (IL-6) is one of the proinflammatory cytokines and is induced by tumor necrosis factor-α (TNF-α),[13] Ang II,[14] and other stimuli in vascular smooth muscle cells (VSMCs), endothelial cells, and macrophages. IL-6 plays an

Received November 17, 2008; first decision November 24, 2008; revision accepted February 23, 2009.

From the Departments of Cardiovascular Medicine (Q.T., R.M., T.I., I.I., K.I., H.O., K.Y., K.T., K.S.) and Advanced Therapeutics for Cardiovascular Diseases (T.I., K.T.), Kyushu University Graduate School of Medical Sciences, and Peking University First Hospital (Q.T.), Fukuoka, Japan.

Q.T., R.M., and I.I. contributed equally to this work.

Correspondence to Toshihiro Ichiki, MD, PhD, Department of Cardiovascular Medicine, Kyushu University Graduate School of Medical Sciences, 3-1-1 Maidashi, Higashi-ku, 812-8582 Fukuoka, Japan. E-mail ichiki@cardiol.med.kyushu-u.ac.jp

Hypertension **is available at http://hyper.ahajournals.org** **DOI: 10.1161/HYPERTENSIONAHA.108.126656**

important role in vascular remodeling and was reported to be a useful biomarker in predicting future cardiovascular events.[15]

Telmisartan has been shown to induce differentiation of adipocytes through activation of PPARγ. A recent study showed that telmisartan attenuated hepatic steatosis, inflammation, and fibrosis in a rat model of nonalcoholic steatohepatitis.[16] It was also reported that telmisartan treatment of patients with hypertension and coronary heart disease decreased β2-integrin MAC-1 expression in peripheral lymphocytes independent of Ang II.[17] These data suggest that telmisartan has an anti-inflammatory effect independently of AT1R blocking effect. However, an anti-inflammatory effect of telmisartan on blood vessel is incompletely characterized. Therefore, we tested whether telmisartan inhibits TNF-α–induced IL-6 expression through PPARγ in VSMCs.

Materials and Methods

DMEM was purchased from GIBCO/BRL. FBS was from JRH Biosciences. Recombinant TNF-α was a generous gift from Dainippon-Sumitomo Pharmaceutical Co (Osaka, Japan). Telmisartan was a generous gift from Boehringer Ingelheim (Ingelheim, Germany). Valsartan was purchased from US Pharmacopeia. BSA and GW9662 were purchased from Sigma. Pioglitazone was purchased from LKT Laboratories. [α-^{32}P] dCTP and [γ-^{32}P]ATP were purchased from Perkin-Elmer Life Sciences. Antibodies against extracellular signal-regulated protein kinase (ERK), p38 mitogen-activated protein kinase (MAPK), c-Jun N-terminal kinase (JNK), and their phosphorylated forms were purchased from Cell Signaling Technology. Other reagents were purchased from Wako Pure Chemicals unless otherwise mentioned specifically. TNF-α was dissolved in DMEM with 0.1% BSA, and Ang II was suspended in sterile water. Other reagents that added to culture medium were dissolved in dimethyl sulfoxide at a final concentration of 0.1%, which did not show any effect on IL-6 induction.

Cell Culture

VSMCs were isolated from the thoracic aorta of Sprague–Dawley rats and cultured in a humidified atmosphere of 95% air/5% CO_2 at 37°C in DMEM as described previously.[14] Cells were grown to confluence and growth-arrested in DMEM with 0.1% BSA for 2 days before use. Passages between 5 and 13 were used for the experiments.

Northern Blotting

Total RNA was prepared according to the acid guanidinium thiocyanate-phenol-chloroform extraction method. Northern blot analysis of IL-6 mRNA and 18S ribosomal RNA (rRNA) was performed as described previously.[14] The radioactivity of hybridized bands of IL-6 mRNA and rRNA was quantified with a MacBAS Bioimage Analyzer (Fuji Photo Film). It was reported that 2 species of IL-6 mRNA were generated by an alternative polyadenylation.[18] The intensity of both bands was taken into account for quantification.

Quantification of Rat IL-6 by Sandwich ELISA

VSMCs were stimulated with TNF-α (10 ng/mL) or Ang II (100 nmol/L) for 24 hours in the presence or absence of telmisartan (1 to 20 μmol/L). Then the medium of VSMCs was collected and centrifuged at 12 000 rpm for 1 minute. The supernatant was stored at −70°C until used for the assay. ELISA for rat IL-6 was performed with a Cytoscreen ELISA kit (BioSource International) according to manufacturer instructions. The measurement was performed in duplicate.

Transfection of IL-6 Promoter–Luciferase Fusion DNA Construct to VSMCs

The IL-6 gene promoter–luciferase fusion DNA constructs and luciferase assay were described previously.[14] Detailed protocols can be found in an online data supplement available at http://hyper.ahajournals.org.

Plasmids of NF-κB–luciferase and CCAAT/enhancer-binding protein-β (C/EBPβ)–luciferase were purchased from Stratagene Co. Five copies of NF-κB consensus sequence or 3 copies of C/EBPβ consensus sequence were ligated to minimal promoter followed by luciferase gene.

Gel Mobility Shift Assay

Gel mobility shift assay was performed as described previously[14] using synthetic NF-κB and C/EBPβ DNA probe (NF-κB: CAT GTG GGA TTT TCC CAT GA; C/EBPβ: CAC ATT GCA CAA TCT TAA). Detailed protocols are indicated in the online supplement.

Effect of Telmisartan on Ang II– and TNF-α–Induced IL-6 Production In Vivo

All procedures were approved by the institutional animal use and care committee and were conducted in conformity with institutional guidelines of Kyushu University. Ang II (490 ng/kg per minute) or TNF-α (80 ng/kg per minute) was administered subcutaneously to 9-week-old C57/BL6 mice (Kyudo Co; Saga, Japan) by osmotic mini-pump (Alzet) for 1 week. Doses of TNF-α and Ang II were determined in a preliminary experiment to detect a significant increase in the serum IL-6 level. Telmisartan was dissolved in water (10 μg/mL) and administered ad libitum. The estimated dose of orally ingested telmisartan was 2 mg/kg per day. Blood pressure and heart rate were measured using tail-cuff method (UR-5000; UEDA). After 1 week, mice were euthanized under pentobarbital anesthesia, and peripheral blood was collected from inferior vena cava. The serum concentration of IL-6 was measured using ELISA kit (R&D Systems). No significant differences in body weight were observed among the treatment groups (data not shown).

Ex Vivo Stimulation of Rat Aorta

Nine-week-old Sprague-Dawley rats were purchased from Kyudo Co. Rats were euthanized under deep pentobarbital anesthesia. The aorta was excised and adventitia was removed. The aorta was cut into 6 pieces and stimulated with TNF-α (50 ng/mL) or Ang II (1 μmol/L) in the absence or presence of telmisartan (10 μmol/L) in 500 μL of DMEM supplemented with 0.1% BSA for 48 hours. Concentrations of Ang II and TNF-α were determined in a preliminary experiment to detect a significant increase in the production of IL-6 in the supernatant of ex vivo–cultured aortic segments. The supernatant was subjected to ELISA to measure IL-6 production. The IL-6 concentration in the supernatant was normalized with the wet weight of the aortic segment.

RT-PCR and Western Blot Analysis

Detailed protocols are indicated in the online supplement.

Statistical Analysis

Statistical analysis was performed with 1-way ANOVA and Fisher's test if appropriate. A P value <0.05 was considered statistically significant. Values are expressed as mean±SEM.

Results

Telmisartan Attenuated TNF-α–Induced IL-6 Expression

VSMCs were incubated with or without telmisartan (10 μmol/L) for 60 minutes. Then the cells were stimulated with TNF-α (10 ng/mL) for 30 minutes. Northern blot analysis revealed attenuation of TNF-α–induced IL-6 mRNA expression by telmisartan (Figure 1A). However, valsartan (10 μmol/L), another AT1R antagonist, failed to suppress TNF-α–induced IL-6 mRNA expression (Figure 1B). Telmisartan (1 to 20 μmol/L) dose-dependently suppressed TNF-α–induced IL-6 mRNA expression (Figure 1C). The concentration range of telmisartan was chosen based on a previous

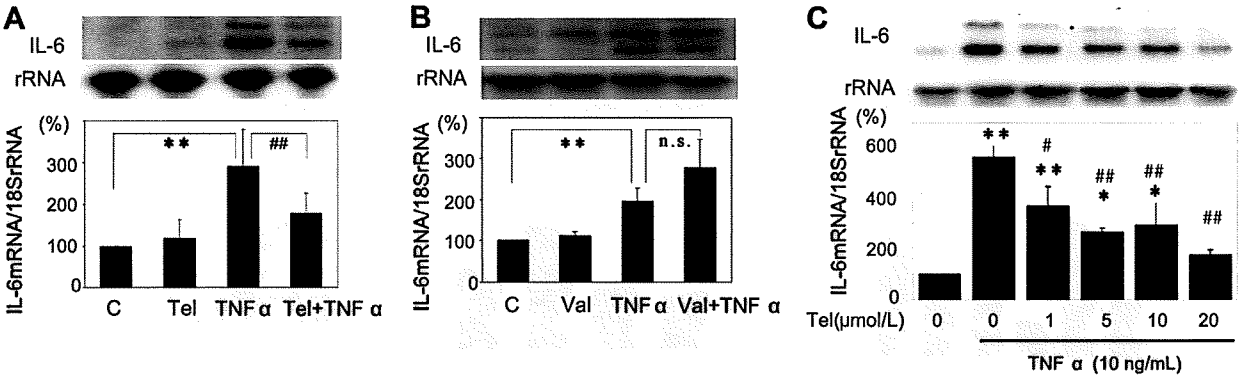

Figure 1. Suppression of TNF-α–induced IL-6 mRNA expression by telmisartan (Tel). VSMCs were preincubated with Tel (10 μmol/L; A), valsartan (Val; 10 μmol/L; B), or various concentrations (1 to 20 μmol/L; C) of telmisartan for 60 minutes and stimulated with TNF-α (10 ng/mL) for 30 minutes. Total RNA was isolated, and expression of IL-6 mRNA and 18S rRNA was determined by Northern blot analysis. Radioactivity of IL-6 mRNA was measured with an imaging analyzer and was normalized by radioactivity of rRNA. Values (mean±SEM) are expressed as percentage of control culture in a bar graph (100%; No. of independent experiments was 5). *P<0.05; **P<0.01 vs control; #P<0.05; ##P<0.01 vs TNF-α.

clinical study[19] that showed that the steady-state serum level of telmisartan was 1 to 5 μmol/L when 80 to 160 mg per day of telmisartan was given for 7 days to patients with essential hypertension. And it was reported that telmisartan at concentrations >25 μmol/L stimulated PPARα.[9] Therefore, we did not use telmisartan at concentrations >20 μmol/L in this study.

The protein level of IL-6 in the supernatant of VSMCs was measured after 24 hours of stimulation with TNF-α (10 ng/mL) with or without preincubation with telmisartan (1 to 20 μmol/L). TNF-α–induced IL-6 protein expression was also dose-dependently attenuated by telmisartan (Figure 2A). Ang II (100 nmol/L)–induced IL-6 production was inhibited completely by telmisartan at lower concentrations (Figure 2B); thus, we confirmed that telmisartan is an effective AT1R antagonist.

We next examined whether telmisartan affected TNF receptor expression. Semiquantitative RT-PCR analysis showed that telmisartan did not affect TNF type 1 receptor mRNA expression (supplemental Figure IB). We could not detect TNF type 2 receptor mRNA in our VSMCs. We also examined the effect of telmisartan on TNF-α–induced MAPK activation (supplemental Figure II). Telmisartan did not affect TNF-α–induced activation of ERK, p38MAPK, or JNK.

Telmisartan Inhibition of TNF-α–Induced IL-6 Expression Was Dependent on PPARγ

To clarify the role of PPARγ in telmisartan inhibition of TNF-α–induced IL-6 expression, the effect of GW9662, a PPARγ-specific antagonist, was examined. Although GW9662 itself did not affect IL-6 mRNA expression, preincubation with GW9662 (10 μmol/L; 3 hours) blocked telmisartan inhibition of TNF-α–induced IL-6 expression (Figure 3A). Pioglitazone (10 μmol/L; preincubation for 1 hour), a full PPARγ agonist, also suppressed the TNF-α–induced IL-6 mRNA expression (Figure 3B).

Telmisartan-Inhibited IL-6 Gene Promoter Activity

Next, the effect of telmisartan on IL-6 gene promoter activity was examined. TNF-α (10 ng/mL) increased IL-6 gene promoter activity by 2-fold. Preincubation with telmisartan (10 μmol/L) significantly inhibited IL-6 gene promoter activity (Figure 4). Deletion analysis of the IL-6 gene promoter suggested that the DNA segment between −150 bp and −27 bp was responsible for the downregulation by telmisartan (Figure 4A) because telmisartan inhibited the luciferase activity in the −150-bp construct, but the −27-bp

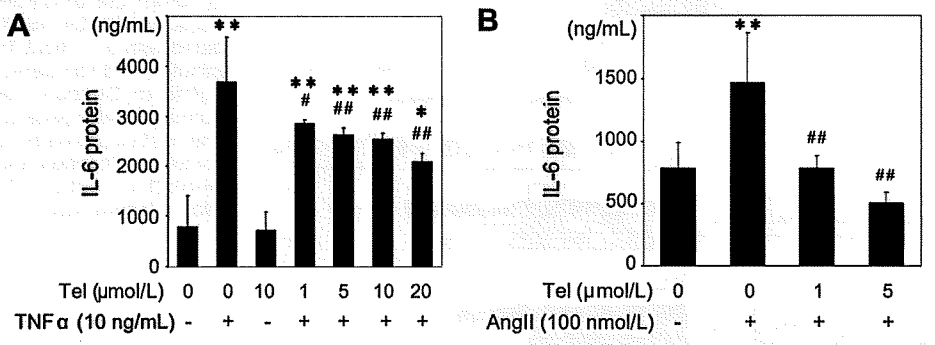

Figure 2. Suppression of TNF-α– and Ang II–induced IL-6 protein production by telmisartan (Tel). A, VSMCs were preincubated with Tel (10 μmol/L) at various concentrations for 60 minutes and stimulated with TNF-α (10 ng/mL) for 24 hours. B, VSMCs were incubated with Tel at 1 or 5 μmol/L and stimulated with Ang II (100 nmol/L) for 24 hours. IL-6 protein production in the supernatant of VSMCs was measured by ELISA. *P<0.05 vs control; **P<0.01 vs control; #P<0.05 vs TNF-α; ##P<0.01 vs TNF-α or Ang II (No. of independent experiment was 6 in duplicate).

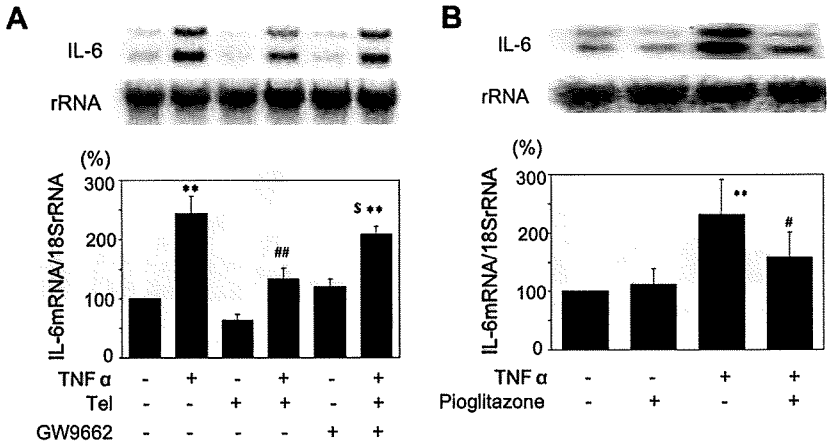

Figure 3. Effect of GW9662 on telmisartan (Tel) inhibition of TNF-α–induced IL-6 expression. A, VSMCs were incubated with GW9662 (10 μmol/L) for 3 hours followed by preincubation with Tel (10 μmol/L) for 60 minutes. Then the VSMCs were stimulated with TNF-α (10 ng/mL) for 30 minutes. B, VSMCs were preincubated with pioglitazone (10 μmol/L) for 60 minutes, then stimulated with TNF-α (10 ng/mL) for 30 minutes. Northern blot analysis of IL-6 mRNA was performed as described in Figure 1 legend. **$P<0.01$ vs control; #$P<0.05$ vs TNF-α; ## $P<0.01$ vs TNF-α; \$$P<0.05$ vs Tel+TNF-α (No. of independent experiments was 4).

construct no longer responded to TNF-α or telmisartan. The DNA segment between −150 bp and −27 bp contains NF-κB and C/EBPβ as consensus cis DNA elements.[20] We therefore examined whether telmisartan inhibited NF-κB– and C/EBPβ-dependent gene transcription activated by TNF-α. As shown in Figure 4B, telmisartan inhibited TNF-α–induced activation of luciferase activity, which is solely dependent on NF-κB or C/EBPβ.

The gel mobility shift assay showed that telmisartan inhibited TNF-α–induced NF-κB DNA binding activity (Figure 5A). Telmisartan also attenuated TNF-α–induced C/EBPβ DNA binding activity to a lesser extent (Figure 5B).

Telmisartan Attenuated IL-6 Production In Vivo and Ex Vivo

To confirm that telmisartan inhibits IL-6 production in vivo, Ang II (490 ng/kg per minute) or TNF-α (80 ng/kg per minute) was administered to mice with or without telmisartan (2 mg/kg per day) for 1 week. Ang II but not TNF-α increased blood pressure level (Table). Ang II–induced high blood pressure was inhibited by telmisartan. Heart rate was not significantly different among the treatment groups. Ang II–induced increase in serum IL-6 level was almost completely inhibited by telmisartan, and telmisartan significantly attenuated TNF-α–induced IL-6 production (Figure 6A). To

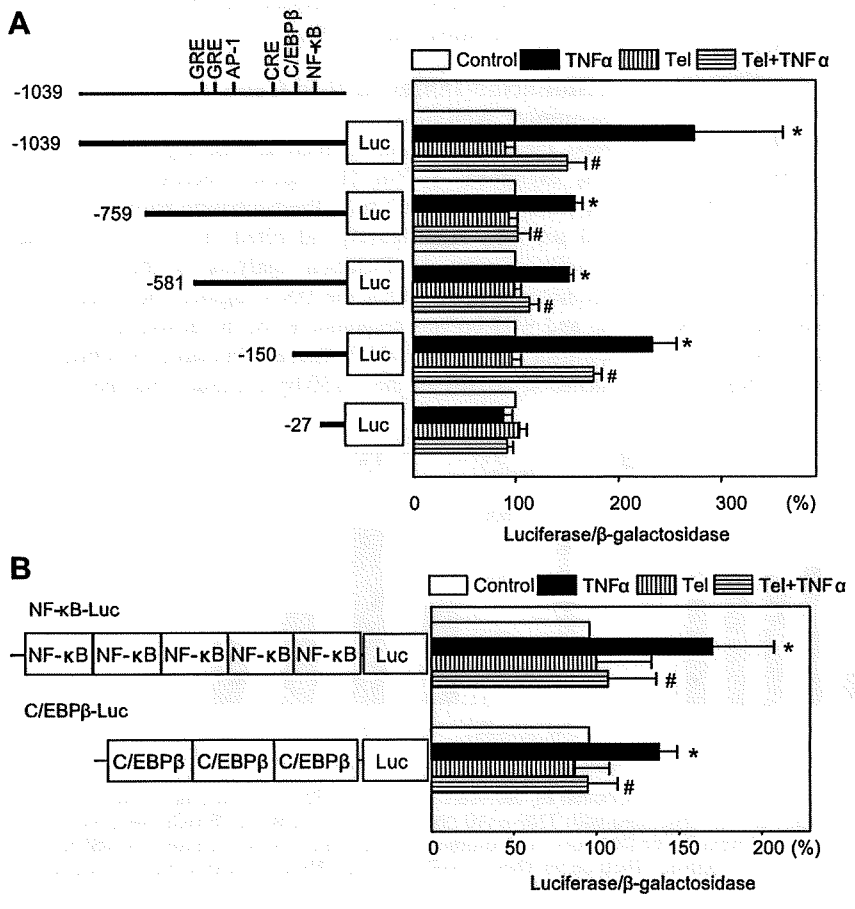

Figure 4. Suppression of IL-6 gene promoter activity by telmisartan (Tel). A, After transfection of IL-6 gene promoter/luciferase (Luc) fusion DNA (5 μg), VSMCs were preincubated with or without Tel (10 μmol/L; 60 minutes) and stimulated with TNF-α (10 ng/mL) for 24 hours. AP-1 indicates activator protein-1. B, NF-κB–Luc or C/EBPβ–Luc was introduced to VSMCs. VSMCs were preincubated with or without Tel (10 μmol/L; 60 minutes) and stimulated with TNF-α (10 ng/mL) for 24 hours. Luc activity was normalized with β-galactosidase activity. The relative promoter activity without stimulation (control) was set as 100%. *$P<0.01$ vs control; #$P<0.05$ vs TNF-α (No. of independent experiments was 4).

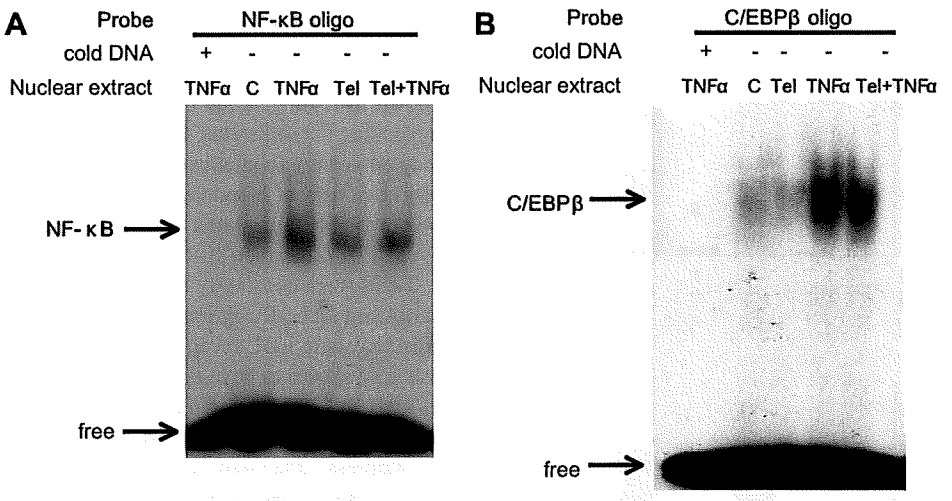

Figure 5. Telmisartan (Tel) attenuated TNF-α–induced NF-κB and C/EBPβ binding. A, Binding activity of NF-κB sequence of IL-6 gene promoter to nuclear extracts from unstimulated (C), TNF-α–stimulated, Tel-stimulated, and Tel- and TNF-α–stimulated VSMCs were examined by gel mobility shift assay. B, Binding activity of C/EBPβ sequence of IL-6 gene promoter to nuclear extracts from unstimulated, Tel-stimulated, TNF-α–stimulated, and Tel- and TNF-α–stimulated VSMCs were examined by gel mobility shift assay. Fifty times molar excess of unlabeled oligonucleotide (oligo) was added to the reaction mixture in the left lane (Cold DNA+). The same results were obtained in other independent experiments (No. of independent experiment was 3).

confirm that IL-6 is produced from blood vessel, a segment of rat aorta without adventitia was stimulated ex vivo with Ang II (1 μmol/L) or TNF-α (50 ng/mL) in the presence or absence of telmisartan (10 μmol/L) for 48 hours. Production of IL-6 induced by TNF-α in the supernatant was significantly attenuated by coincubation with telmisartan (Figure 6B). Ang II–induced production of IL-6 was completely inhibited by telmisartan. These results were consistent with those obtained during in vitro experiments.

Discussion

In the present study, we demonstrated that telmisartan but not valsartan suppressed TNF-α–induced IL-6 expression through a PPARγ-dependent manner. Inhibition of NF-κB and C/EBPβ DNA binding activity by telmisartan may be responsible for attenuation of TNF-α–induced IL-6 expression. This is the first study demonstrating that telmisartan modulates cytokine production induced by non–Ang II stimulus. The in vivo and ex vivo results were consistent with those obtained from the in vitro study. The in vivo study showed that telmisartan had an anti-inflammatory effect in mice, and the ex vivo study indicated that IL-6 was produced from blood vessel in response to TNF-α stimulation, and telmisartan attenuated the induction.

On activation by ligands, PPARγ regulates expression of several genes involved in lipid and carbohydrate metabolism and inflammatory responses.[21] PPARγ regulates gene expression through 2 different transcriptional regulatory mechanisms: transactivation and transrepression. Transactivation depends on PPARγ response element. On activation, PPARγ forms a heterodimer with retinoid X receptor and binds to PPARγ response element in the promoter region of the target genes.[22] In contrast, transrepression involves an interference with other transcription factors such as NF-κB and activator protein 1.[22] Although telmisartan was reported to be a partial agonist of PPARγ, it has not been determined whether telmisartan regulates gene expression through transrepression mechanism. Our data suggest that telmisartan may have a transrepression effect on gene expression in addition to AT1R blockade.

The mechanism of transrepression by PPARγ activators is less well known. A recent study showed that PPARγ activation by TZD induced sumoylation of PPAR, resulting in retention of nuclear receptor corepressor/histone deacetylase complex to the promoter and suppression of gene transcription.[12] Troglitazone, another TZD, inhibited TNF-α–induced and NF-κB–dependent gene transcription without affecting NF-κB nuclear translocation or DNA binding in adipocytes,[23] which may support the above-mentioned model. However, a previous study showed that TZDs inhibited IL-1β–activated NF-κB and C/EBPβ DNA binding to the IL-6 gene promoter.[24] It was also reported that troglitazone inhibited TNF-α–induced IL-6 expression in multiple myeloma cells by inhibiting NF-κB and C/EBPβ DNA binding.[25] In this study, activated PPARγ competed for PPARγ coactivator-1, a transcription coactivator, with NF-κB, resulting in attenua-

Table. Heart Rate and Blood Pressure of Ang II– and TNF-α–Treated Mice

Variable	Control	Tel	Ang II	Tel+Ang II	TNF-α	Tel+TNF-α
HR (bpm)	576±24	598±21	599±18	608±27	611±47	586±22
BP (mm Hg)	95.3±1.3	94.0±2.8	109.6±4.7*	102.2±1.8†	97.3±0.9	95.5±1.4

HR indicates heart rate; BP, blood pressure.
*$P<0.05$ vs control; †$P<0.05$ vs Ang II; n=5.

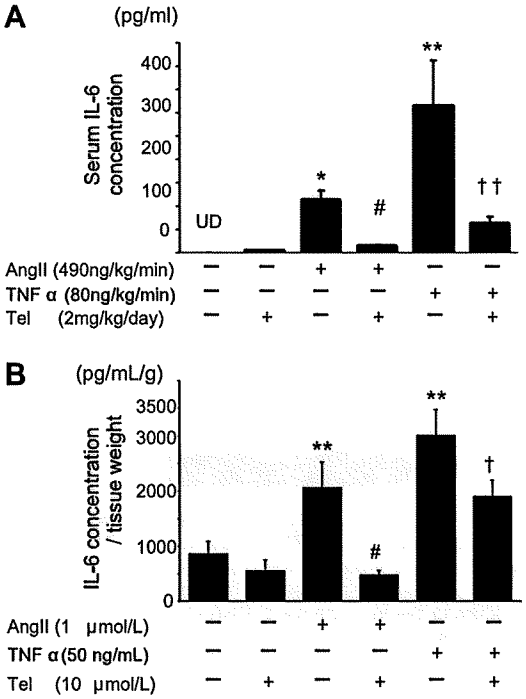

Figure 6. Telmisartan attenuated IL-6 production in vivo and ex vivo. A, Serum concentration of IL-6 was measured in mice injected with Ang II (490 ng/kg per minute) or TNF-α (80 ng/kg per minute) in the presence or absence of telmisartan (Tel; 2 mg/kg per day) administration for 1 week (No. of independent experiments was 5). *P<0.05; **P<0.01 vs control (no treatment); #P<0.05 vs Ang II; ††P<0.01 vs TNF-α. UD indicates undetectable. B, An aortic segment was stimulated ex vivo with Ang II (1 μmol/L) or TNF-α (50 ng/mL) in the presence or absence of Tel (10 μmol/L) in DMEM supplemented with 0.1% BSA for 48 hours. The concentration of IL-6 in the supernatant was measured and normalized with wet weight of the aortic segment (No. of independent experiment was 4 in duplicate). **P<0.01 vs control; #P<0.05 vs Ang II; †P<0.05 vs TNF-α.

tion of TNF-α–induced NF-κB DNA binding. In contrast, activated PPARγ physically interacted with C/EBPβ, suggesting that this protein–protein interaction attenuates the DNA binding of C/EBPβ. Although the precise mechanisms are not clear at this point, it may be possible that telmisartan inhibits NF-κB and C/EBPβ DNA binding activity through the same mechanism.

Inflammation plays a crucial role in the initiation and progression of atherosclerosis.[26] IL-6 enhanced VSMC growth induced by platelet-derived growth factor.[27] IL-6 also increased both monocyte chemoattractant protein-1 production and DNA synthesis of VSMCs, which may coordinate inflammatory and proliferative responses.[28] IL-6 is also a useful biomarker predicting future cardiovascular events.[29] TNF-α also enhances vascular inflammation. Blockade of TNF-α activity by soluble TNF-α receptor suppressed coronary artery neointimal formation after cardiac transplantation in rabbits.[30] Therefore, telmisartan inhibition of TNF-α–induced IL-6 expression, which was not observed by valsartan, may attenuate vascular inflammation.

A recent report showed that C/EBPβ was involved in IL-17–induced C-reactive protein expression in VSMCs.[31] Another report showed that C/EBPβ regulated monocyte chemoattractant protein-1 expression in the aorta of hyperinsulinemic rats.[32] These studies suggest that C/EBPβ is also involved in vascular inflammation. Because NF-κB is well known to regulate gene expression of various inflammatory molecules,[33] telmisartan inhibition of NF-κB and C/EBPβ may contribute to attenuation of a broad range of inflammatory responses of blood vessel. However, it is not clear at this point whether telmisartan modulates gene expression induced by TNF-α other than IL-6 induction.

TZDs were constantly reported to inhibit atherogenesis in various models. Rosiglitazone inhibited development of atherosclerosis in LDL receptor–deficient mice.[11] Rosiglitazone was also shown to have additive effects on plaque regression in the combination treatment with simvastatin in an atherosclerotic rabbit model.[34] AT1R antagonists were also reported to suppress atherogenesis. Strawn et al demonstrated that losartan attenuated atherogenesis in monkeys with hypercholesterolemia.[35] Based on these studies and our results, telmisartan may be more protective against vascular lesion formation attributable to PPARγ activation and AT1R antagonism.

Perspective

In the present study, we showed that telmisartan inhibited Ang II– as well as TNF-α–induced IL-6 expression in VSMCs, rat aorta, and mice. Inhibition of TNF-α–induced IL-6 expression was mediated by PPARγ. And inhibition of NF-κB and C/EBPβ DNA binding by telmisartan may be responsible for suppression of TNF-α–induced IL-6 expression. The dual inhibition (Ang II– and TNF-α–induced IL-6 expression) of the inflammatory cytokine production by telmisartan may be beneficial for treatment of not only hypertension but also atherosclerotic cardiovascular diseases. However, large clinical trials are needed to determine whether these unique properties of telmisartan cause better clinical outcome in cardiovascular disease prevention.

Sources of Funding

This study was supported in part by grants-in-aid for scientific research from the Ministry of Education, Culture, Sports, Science and Technology of Japan (19590867; T.I.). Q.T. was supported by the Japan–China Sasakawa Medical Fellowship.

Disclosures

None.

References

1. de Gasparo M, Catt KJ, Inagami T, Wright JW, Unger T. International union of pharmacology. XXIII. The angiotensin II receptors. *Pharmacol Rev.* 2000;52:415–472.
2. Ferrario CM. Role of angiotensin II in cardiovascular disease therapeutic implications of more than a century of research. *J Renin Angiotensin Aldosterone Syst.* 2006;7:3–14.
3. McMurray JJ, Ostergren J, Swedberg K, Granger CB, Held P, Michelson EL, Olofsson B, Yusuf S, Pfeffer MA. Effects of candesartan in patients with chronic heart failure and reduced left-ventricular systolic function taking angiotensin-converting-enzyme inhibitors: the CHARM-Added trial. *Lancet.* 2003;362:767–771.
4. Barnett AH, Bain SC, Bouter P, Karlberg B, Madsbad S, Jervell J, Mustonen J. Angiotensin-receptor blockade versus converting-enzyme inhibition in type 2 diabetes and nephropathy. *N Engl J Med.* 2004;351:1952–1961.

5. Pfeffer MA, McMurray JJ, Velazquez EJ, Rouleau JL, Kober L, Maggioni AP, Solomon SD, Swedberg K, Van de Werf F, White H, Leimberger JD, Henis M, Edwards S, Zelenkofske S, Sellers MA, Califf RM. Valsartan, captopril, or both in myocardial infarction complicated by heart failure, left ventricular dysfunction, or both. *N Engl J Med.* 2003; 349:1893–1906.
6. Gillespie EL, White CM, Kardas M, Lindberg M, Coleman CI. The impact of ACE inhibitors or angiotensin II type 1 receptor blockers on the development of new-onset type 2 diabetes. *Diabetes Care.* 2005;28: 2261–2266.
7. Healey JS, Baranchuk A, Crystal E, Morillo CA, Garfinkle M, Yusuf S, Connolly SJ. Prevention of atrial fibrillation with angiotensin-converting enzyme inhibitors and angiotensin receptor blockers: a meta-analysis. *J Am Coll Cardiol.* 2005;45:1832–1839.
8. Schupp M, Janke J, Clasen R, Unger T, Kintscher U. Angiotensin type 1 receptor blockers induce peroxisome proliferator-activated receptor-gamma activity. *Circulation.* 2004;109:2054–2057.
9. Benson SC, Pershadsingh HA, Ho CI, Chittiboyina A, Desai P, Pravenec M, Qi N, Wang J, Avery MA, Kurtz TW. Identification of telmisartan as a unique angiotensin II receptor antagonist with selective PPARgamma-modulating activity. *Hypertension.* 2004;43:993–1002.
10. Yki-Jarvinen H.Thiazolidinediones. *N Engl J Med.* 2004;351:1106–1118.
11. Li AC, Brown KK, Silvestre MJ, Willson TM, Palinski W, Glass CK. Peroxisome proliferator-activated receptor gamma ligands inhibit development of atherosclerosis in LDL receptor-deficient mice. *J Clin Invest.* 2000;106:523–531.
12. Pascual G, Fong AL, Ogawa S, Gamliel A, Li AC, Perissi V, Rose DW, Willson TM, Rosenfeld MG, Glass CK. A SUMOylation-dependent pathway mediates transrepression of inflammatory response genes by PPAR-gamma. *Nature.* 2005;437:759–763.
13. Wang Z, Castresana MR, Newman WH. NF-kappaB is required for TNF-alpha-directed smooth muscle cell migration. *FEBS Lett.* 2001;508: 360–364.
14. Funakoshi Y, Ichiki T, Ito K, Takeshita A. Induction of interleukin-6 expression by angiotensin II in rat vascular smooth muscle cells. *Hypertension.* 1999;34:118–125.
15. Lobbes MB, Lutgens E, Heeneman S, Cleutjens KB, Kooi ME, van Engelshoven JM, Daemen MJ, Nelemans PJ. Is there more than C-reactive protein and fibrinogen? The prognostic value of soluble CD40 ligand, interleukin-6 and oxidized low-density lipoprotein with respect to coronary and cerebral vascular disease. *Atherosclerosis.* 2006;187:18–25.
16. Fujita K, Yoneda M, Wada K, Mawatari H, Takahashi H, Kirikoshi H, Inamori M, Nozaki Y, Maeyama S, Saito S, Iwasaki T, Terauchi Y, Nakajima A. Telmisartan, an angiotensin II type 1 receptor blocker, controls progress of nonalcoholic steatohepatitis in rats. *Dig Dis Sci.* 2007;52:3455–3464.
17. Link A, Lenz M, Legner D, Böhm M, Nickenig G. Telmisartan inhibits beta2-integrin MAC-1 expression in human T-lymphocytes. *J Hypertens.* 2006;24:1891–1898.
18. Northemann W, Braciak TA, Hattori M, Lee F, Fey GH. Structure of the rat interleukin 6 gene and its expression in macrophage-derived cells. *J Biol Chem.* 1989;264:16072–16082.
19. Stangier J, Su CA, Roth W. Pharmacokinetics of orally and intravenously administered telmisartan in healthy young and elderly volunteers and in hypertensive patients. *J Int Med Res.* 2000;28:149–167.
20. Dendorfer U, Oettgen P, Libermann TA. Multiple regulatory elements in the interleukin-6 gene mediate induction by prostaglandins, cyclic AMP, and lipopolysaccharide. *Mol Cell Biol.* 1994;14:4443–4454.
21. Brown JD, Plutzky J. Peroxisome proliferator-activated receptors as transcriptional nodal points and therapeutic targets. *Circulation.* 2007;115: 518–533.
22. Glass CK, Ogawa S. Combinatorial roles of nuclear receptors in inflammation and immunity. *Nat Rev Immunol.* 2006;6:44–55.
23. Ruan H, Pownall HJ, Lodish HF. Troglitazone antagonizes tumor necrosis factor-alpha-induced reprogramming of adipocyte gene expression by inhibiting the transcriptional regulatory functions of NF-kappaB. *J Biol Chem.* 2003;278:28181–28192.
24. Takata Y, Kitami Y, Yang ZH, Nakamura M, Okura T, Hiwada K. Vascular inflammation is negatively autoregulated by interaction between CCAAT/enhancer-binding protein-delta and peroxisome proliferator-activated receptor-gamma. *Circ Res.* 2002;91:427–433.
25. Wang LH, Yang XY, Zhang X, Farrar WL. Inhibition of adhesive interaction between multiple myeloma and bone marrow stromal cells by PPARgamma crosstalk with NF-kappaB and c/EBPbeta. *Blood.* 2007; 110:4373–4384.
26. Ross R. Atherosclerosis–an inflammatory disease. *N Engl J Med.* 1999; 340:115–126.
27. Ikeda U, Ikeda M, Oohara T, Oguchi A, Kamitani T, Tsuruya Y, Kano S. Interleukin 6 stimulates growth of vascular smooth muscle cells in a PDGF-dependent manner. *Am J Physiol.* 1991;260:H1713–H1717.
28. Watanabe S, Mu W, Kahn A, Jing N, Li JH, Lan HY, Nakagawa T, Ohashi R, Johnson RJ. Role of JAK/STAT pathway in IL-6-induced activation of vascular smooth muscle cells. *Am J Nephrol.* 2004;24: 387–392.
29. Koenig W, Khuseyinova N. Biomarkers of atherosclerotic plaque instability and rupture. *Arterioscler Thromb Vasc Biol.* 2007;27:15–26.
30. Clausell N, Molossi S, Sett S, Rabinovitch M. In vivo blockade of tumor necrosis factor-alpha in cholesterol-fed rabbits after cardiac transplant inhibits acute coronary artery neointimal formation. *Circulation.* 1994; 89:2768–2779.
31. Patel DN, King CA, Bailey SR, Holt JW, Venkatachalam K, Agrawal A, Valente AJ, Chandrasekar B. Interleukin-17 stimulates C-reactive protein expression in hepatocytes and smooth muscle cells via p38 MAPK and ERK1/2-dependent NF-kappaB and C/EBPbeta activation. *J Biol Chem.* 2007;282:27229–27238.
32. Sato Y, Nishio Y, Sekine O, Kodama K, Nagai Y, Nakamura T, Maegawa H, Kashiwagi A. Increased expression of CCAAT/enhancer binding protein-beta and -delta and monocyte chemoattractant protein-1 genes in aortas from hyperinsulinaemic rats. *Diabetologia.* 2007;50:481–489.
33. de Winther MP, Kanters E, Kraal G, Hofker MH. Nuclear factor kappaB signaling in atherogenesis. *Arterioscler Thromb Vasc Biol.* 2005;25: 904–914.
34. Phillips JW, Barringhaus KG, Sanders JM, Yang Z, Chen M, Hesselbacher S, Czarnik AC, Ley K, Nadler J, Sarembock IJ. Rosiglitazone reduces the accelerated neointima formation after arterial injury in a mouse injury model of type 2 diabetes. *Circulation.* 2003;108: 1994–1999.
35. Strawn WB, Chappell MC, Dean RH, Kivlighn S, Ferrario CM. Inhibition of early atherogenesis by losartan in monkeys with diet-induced hypercholesterolemia. *Circulation.* 2000;101:1586–1593.

Soluble Flt-1 Gene Transfer Ameliorates Neointima Formation After Wire Injury in flt-1 Tyrosine Kinase–Deficient Mice

Jun-ichiro Koga, Tetsuya Matoba, Kensuke Egashira, Mitsuki Kubo, Miho Miyagawa, Eiko Iwata, Katsuo Sueishi, Masabumi Shibuya, Kenji Sunagawa

Objective—We have demonstrated that vascular endothelial growth factor (VEGF) expression is upregulated in injured vascular wall, and blockade of VEGF inhibited monocyte infiltration and neointima formation in several animal models. In the present study, we aimed to clarify relative role of two VEGF receptors, flt-1 versus flk-1/KDR, in neointima formation after injury using flt-1 tyrosine kinase-deficient (Flt-1 $TK^{-/-}$) mice and soluble Flt-1(sFlt-1) gene transfer.

Methods and Results—Neointima formation was comparable between wild-type and Flt-1 $TK^{-/-}$ mice 28 days after intraluminal wire injury in femoral arteries. By contrast, neointima formation was significantly suppressed by sFlt-1 gene transfer into Flt-1 $TK^{-/-}$ mice that blocks VEGF action on flk-1 (intima/media ratio: 2.8 ± 0.4 versus 1.4 ± 0.4, $P<0.05$). The inhibition of neointima formation was preceded by significant reduction of monocyte chemoattractant protein (MCP-1) expression in vascular smooth muscle cells (VSMCs) and monocyte infiltration 7 days after injury. Gene transfer of sFlt-1 or treatment of flk-1–specific antibody significantly inhibited VEGF-induced MCP-1 expression determined by RT-PCR in cultured aortic tissue and VSMCs. MCP-1–induced chemotaxis was equivalent between wild-type and Flt-1 $TK^{-/-}$ mice.

Conclusions—These results suggest that endogenous VEGF accelerates neointima formation through flk-1 by regulating MCP-1 expression in VSMCs and macrophage-mediated inflammation in injured vascular wall in murine model of wire injury. (***Arterioscler Thromb Vasc Biol.* 2009;29:458-464.**)

Key Words: restenosis ■ inflammation ■ smooth muscle cells ■ angiogenesis

Vascular endothelial growth factor (VEGF) is one of the most potent angiogenic and vascular permeability factors playing essential roles in neonatal and postnatal vascular formation. VEGF has gathered growing attention because of its possible contribution to cardiovascular pathophysiology including therapeutic angiogenesis, endothelial regeneration, and inflammation in the vascular wall. VEGF expression is upregulated in human coronary arterial wall after stent implantation, suggesting its role in reendothelialization, perivascular angiogenesis, and neointima formation leading to clinical restenosis.[1] VEGF induction is reproduced in various animal vascular injury models including wire or cuff injury in mice, and balloon injury in rats and rabbits, porcine coronary stent model.[2–4] From these prior studies that supplement or inhibit VEGF pathway in animal models, two conflicting mechanisms have been demonstrated in which VEGF may contribute to neointima formation. One is that VEGF inhibits neointima formation by promoting reendothelialization and inhibiting vascular smooth muscle cell (VSMC) proliferation.[5] The other is that VEGF accelerates neointima formation by promoting inflammation[2,4] and adventitial angiogenesis in the vascular wall.[2,3,6]

In this controversy, clinical studies have been carried out to examine the effect of VEGF gene delivery after percutaneous coronary angioplasty without significant reduction in restenosis.[7–9] Thus, it is crucial to understand the mechanisms underlying differential effects of VEGF during neointima formation to optimize vasculoprotective effects and minimize adverse effects of endogenous VEGF that may depend on receptor, cell type, and the mode of vascular injury including species studied. We have demonstrated that flt-1 (VEGF receptor 1) is upregulated during neointima formation after vascular injury, especially in the neointima, media, and adventitia, and flk-1/KDR (VEGF receptor 2) in the neointima and media, and that blockade of VEGF by soluble Flt-1 (sFlt-1) gene transfer inhibited monocyte infiltration and neointima formation in several animal models.[2,4] However, contribution of each VEGF receptor was not fully clarified in

Received December 2, 2007; revision accepted January 7, 2009.

From the Department of Cardiovascular Medicine (J.K., T.M., K.E., M.K., M.M., E.I., K. Sunagawa) and the Division of Pathophysiological and Experimental Pathology (K. Sueishi), Graduate School of Medical Sciences, Kyushu University, Fukuoka, Japan; and the Department of Molecular Oncology (M.S.), Graduate School of Medicine and Dentistry, Tokyo Medical and Dental University, Tokyo, Japan.

Correspondence to Kensuke Egashira, MD, PhD, Department of Cardiovascular Medicine, Graduate School of Medical Sciences, Kyushu University, 3-1-1, Maidashi, Higashi-ku, Fukuoka 812-8582, Japan. E-mail egashira@cardiol.med.kyushu-u.ac.jp

Arterioscler Thromb Vasc Biol **is available at http://atvb.ahajournals.org** **DOI: 10.1161/ATVBAHA.109.183772**

previous studies including ours, because sFlt-1 as well as other VEGF traps sequesters VEGF from its receptors nonspecifically.[2,10] It is reported that flk-1/KDR mainly mediates endothelial cell proliferation during angiogenesis,[11] so that flk-1 may promote reendothelialization and suppress neointima formation after injury. By contrast, flt-1 is reported to regulate nitric oxide production in endothelial cells,[12] and to regulate monocyte chemotaxis that may promote inflammation and influence neointima formation.[13] Therefore, the present study aimed to determine the relative role of each VEGF receptor, flt-1 versus flk-1, in neointima formation after vascular injury, using flt-1 tyrosine kinase-deficient (Flt-1 $TK^{-/-}$) mice[14] in the presence or absence of sFlt-1 gene transfer[2,15] in wire injury model.

Methods

Experimental Animals

All study protocols were reviewed and approved by the Committee on the Ethics of Animal Experiments in Kyushu University Graduate School of Medical Sciences. To examine the role of flt-1, we used Flt-1 $TK^{-/-}$ mice on C57Bl/6J background because flt-1 deficiency is known to be embryonic lethal.[14] Age-matched C57Bl/6J mice (CLEA Japan, Tokyo, Japan) were used as wild-type (WT) control. All mice were fed with normal diet and water at libitum.

Expression Vector

The 3.3-kb mouse *sFLT-1* gene, originally cloned from mouse lung cDNA library, was subcloned into the *Bam*H I (5′) and *Not* I (3′) sites of the eukaryotic expression vector cDNA3 plasmid (Invitrogen, Carlsbad, Calif).[2,16]

Femoral Arterial Wire Injury

To examine the role of flt-1 in neointima formation, femoral arterial wire injury was performed in male 12- to 20-week-old WT or Flt-1 $TK^{-/-}$ mice. After exposure of left femoral artery, straight spring wire (0.38 mm in diameter, COOK) was inserted into femoral artery from the muscular branch. The wire was placed for 1 minute to denude and dilate the artery. After removal of wire, branch artery was ligated and restoration of blood flow was verified by pulsation of peripheral arteries.[2,17] Twenty-eight days after injury, femoral artery was excised after injection of 10% buffered formalin and evaluated histopathologically. Heart rate and systolic blood pressure were measured by tail cuff method before sacrifice.

Soluble Flt-1 Gene Transfer

To examine the role of flk-1, sFlt-1 gene transfer was performed in Flt-1 $TK^{-/-}$ mice as described elsewhere.[2,4,15] Briefly, plasmid vector encoding sFlt-1 cDNA (100 μg) was injected in the gastrocnemial muscle followed by electroporation to facilitate gene transfer. sFlt-1 gene transfer was performed once every 2 weeks from 14 days before until 28 days after injury, based on the data that serum sFlt-1 concentration was elevated over 28 days after single injection of sFlt-1 plasmid with the peak at 14 day after injection (serum sFlt-1concentration at baseline and 3, 14, and 28 days after injection was 222±24, 396±59,* 970±55,* and 477±54* pg/mL, *$P<0.05$ versus baseline).

Histopathology and Immunohistochemistry

For histopathologic and immunohistochemical analysis, serial paraffin sections of the femoral artery were prepared. Briefly, femoral artery was excised after perfusion of 10% buffered formalin and fixed overnight in formalin. After fixation, the tissue was embedded in paraffin and cross sections (6 μm thick) were stained with Masson trichrome or elastica van Gieson stains. Neointima area was defined as the area surrounded by internal elastic lamina except lumen area. Extent of neointima formation was evaluated by the areal ratio of intima to media (I/M ratio) and neointima area. Other sections were subjected to immunostaining using rat anti-mouse macrophage monoclonal antibodies (Mac-3; BD Pharmingen), goat antimouse monocyte chemoattractant protein-1 (MCP-1) antibodies (Santa Cruz Biotechnology Inc). Proliferating cells were evaluated by the immunostaining with antiproliferating cell nuclear antigen (PCNA) antibody (DAKO). Alpha-smooth muscle actin (α-SMA, DAKO) and CD31 antibody (Santa Cruz) were also used as smooth muscle and endothelium marker. The respective nonimmune IgGs were used as negative controls. After incubation with biotinylated goat antirat IgG (Santa Cruz Biotechnology Inc) or rabbit anti-goat IgG (Nichirei), the sections were incubated with diaminobenzidine (DAB). The sections were then counterstained with Mayer hematoxylin. Analysis was performed using a microscope with a computerized, digital image analysis system and Scion Image Software (Scion Corporation). Fluorescent immunostaining was performed with secondary antibodies which are labeled by AlexaFluor 488 or 555 (Invitrogen).

Ex Vivo Culture of Mouse Aorta

Male 12- to 20-week-old WT Flt-1 $TK^{-/-}$ and sFlt-1 plasmid-injected Flt-1 $TK^{-/-}$ mice were used in this experiment. In the first experiment, sFlt-1 plasmid was injected 7 days before excision of aorta. Aorta was excised from ascending aorta to the bifurcation of iliac arteries and incubated with Dulbecco modified Eagle medium (DMEM) containing 1% fetal bovine serum (FBS). After overnight starvation, aorta was incubated with 50 ng/mL VEGF for 3 hours. Then, mRNA was extracted and quantitative real-time RT-PCR was performed by ABI PRISM 7000 Sequence Detection System (Applied Biosystems). MCP-1 and GAPDH primer, which is mixed with probes as TaqMan Gene Expression Assays, were commercially available and purchased from Applied Biosystems. The second experiment was performed using WT mice and blocking antibody of flt-1(R&D Systems Inc) and flk-1 (R&D Systems Inc). After overnight incubation with these antibodies, mRNA was collected in a similar fashion.

VEGF-Induced MCP-1 Expression in VSMCs

Mouse aortic VSMCs (P53LMACO1)[18] was purchased from Health Science Research Resource Banks and cultured in DMEM containing 10% FBS and phorbol-12myristate-13acetate (PMA, 100 nmol/L). VSMCs were used after 9 passages in the experiment. VSMCs were starved overnight and incubated with blocking antibody for flt-1 (10 μg/mL, R&D Systems) or flk-1 (1 μg/mL, R&D Systems). MCP-1 gene expression was analyzed by real-time PCR after 4-hour stimulation with 200 ng/mL human VEGF.

Peritoneal Macrophage Chemotaxis

Peritoneal fluid containing macrophage was harvested 4 days after intraperitoneal injection of thioglycolate. Macrophage migration was measured in 96-well chemotaxis chambers (Neuro Probe Inc). MCP-1 or VEGF in RPMI 1640 was added to the lower wells and the isolated macrophages (1×10^7 cells per mL) were placed in the upper wells. The concentration of MCP-1 and VEGF was 5, 15, and 50 ng/mL. After incubation for 90 minutes at 37°C, the upper surface of the membrane was washed with PBS and migrated cells on the lower surface were counted after staining with trypan blue. The number of cells per field was counted. All assays were performed in triplicate.

Statistics

All data are reported as the mean±SE. Statistical analysis of differences was performed by Student *t* test and 1-way ANOVA with Bonferroni post test. Statistical analysis of chemotaxis assay was performed by 2-way ANOVA with Bonferroni post test. Probability values less than 0.05 were considered to be statistically significant.

Results

Distinct Role of flt-1 and flk-1 in Neointima Formation After Wire Injury

To examine the role of flt-1 in neointima formation, we examined the degree of neointima formation after wire injury

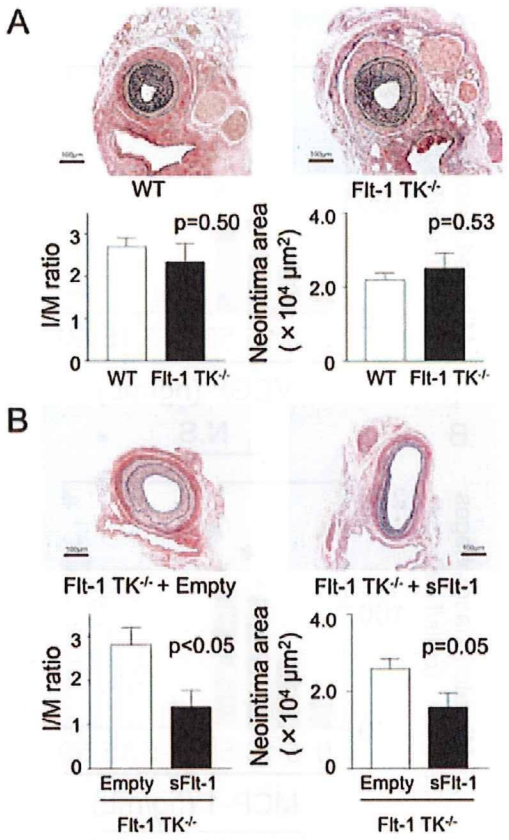

Figure 1. Distinct effects of flt-1 TK deficiency and sFlt-1 gene transfer on neointima formation. Neointima formation was comparable in wild-type (WT, n=7) and Flt-1 $TK^{-/-}$ mice (n=8) 28 days after wire injury (A). Neointima formation was significantly inhibited in Flt-1 $TK^{-/-}$ mice transfected with sFlt-1 plasmid (n=6) compared with empty plasmid (Empty, n=6; B). Scale bar indicates 100 μm.

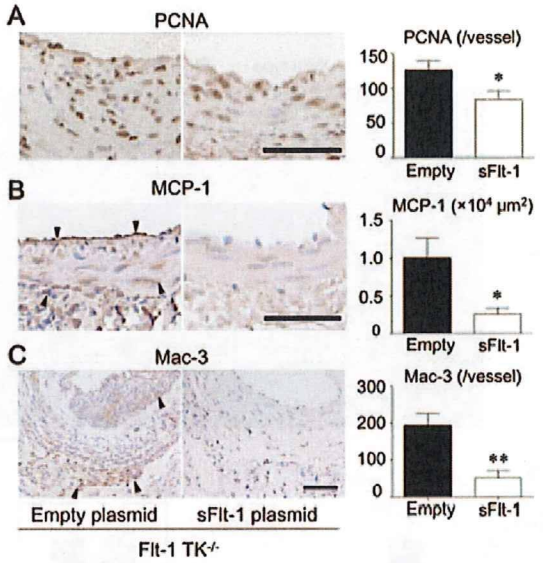

Figure 2. Gene transfer of sFlt-1 in Flt-1 $TK^{-/-}$ mice decreased PCNA-positive cells in the neointima (A), MCP-1 expression in the endothelial layer and medial cells (B), and Mac-3–positive monocytes/macrophages in the neointima and the adventitia (C) 7 days after injury (n=5 to 6 for each group). Scale bar indicate 50 μm. *$P<0.05$, **$P<0.01$ vs empty plasmid group. Arrowheads (▼) indicates stained cells.

in femoral arteries of Flt-1 $TK^{-/-}$ mice. Flt-1 $TK^{-/-}$ mice lack intracellular tyrosine kinase domain of flt-1 and thus downstream signaling.[14] Histological analysis revealed that there was no significant difference in I/M ratio and neointimal area 28 days after wire injury between WT and Flt-1 $TK^{-/-}$ mice (Figure 1A), suggesting that the role of flt-1 is minor in neointima formation in this model. Deficiency of flt-1 tyrosine kinase unaffected heart rate (673±11 versus 662±19 bpm) or blood pressure (110±3 versus 104±3 mm Hg) in mice, also unaffected macrophage infiltration evaluated as mac-3 staining, perivascular fibrosis and vessel diameter (data not shown).

To examine the role of flk-1, sFlt-1 gene transfer was performed into Flt-1 $TK^{-/-}$ mice. The sFlt-1 sequesters VEGF from both VEGF receptors and thus we could evaluate the role of flk-1 when applied to Flt-1 $TK^{-/-}$ mice. The sFlt-1 gene transfer markedly inhibited neointima formation with significant reduction of I/M ratio compared with control empty plasmid in Flt-1 $TK^{-/-}$ mice (Figure 1B). The sFlt-1 gene transfer did not affect heart rate (662±19 versus 660±11 bpm) and blood pressure (95±5 versus 107±4 mm Hg) in Flt-1 $TK^{-/-}$ mice.

sFlt-1 Gene Transfer Suppressed Proliferation, Monocyte Infiltration, and MCP-1 Expression in Flt-1 $TK^{-/-}$ Mice

We have repeatedly shown the importance of MCP-1 and monocyte-mediated inflammation in the vascular wall during vascular remodeling in various vascular disease models.[19–22] Thus, we analyzed the effect of sFlt-1 gene transfer on proliferation of vascular wall cells, MCP-1 expression, and monocyte/macrophage infiltration at an early stage of neointima formation. Histology at 7 days after injury showed a decrease in PCNA-positive cells in the neointima of Flt-1 $TK^{-/-}$ mice transfected with sFlt-1 gene that underpins reduction in neointima formation (Figure 2A). Prominent MCP-1 induction was found in the intimal and the medial cells in Flt-1 $TK^{-/-}$ mice, which was markedly suppressed by sFlt-1 gene transfer (Figure 2B). Infiltration of Mac-3–positive monocytes was found in the media and adventitia, which was suppressed by sFlt-1 gene transfer as well (Figure 2C). These results suggest that endogenous VEGF upregulates MCP-1 and macrophage recruitment via flk-1 in Flt-1 $TK^{-/-}$ mice during neointima formation after wire injury.

Distinct Role of flt-1 and flk-1 in VEGF-Mediated MCP-1 Induction

To elucidate detailed mechanisms of VEGF-mediated MCP-1 induction in injured arteries, we first performed double immunostaining of MCP-1 and α-SMA 3 days after injury when the endothelium has not regenerated yet. We found equivalent MCP-1 induction in the medial VSMCs in WT and Flt-1 $TK^{-/-}$ mice. In contrast, sFlt-1 gene transfer into Flt-1 $TK^{-/-}$ mice remarkably inhibited MCP-1 induction (Figure 3A). These results suggest that (1) wire injury induces MCP-1 expression primarily in the VSMCs and (2) flk-1, but not

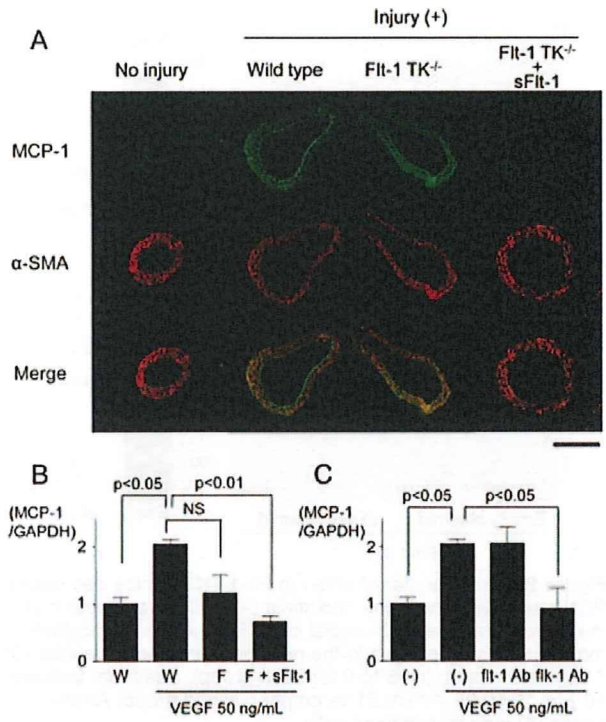

Figure 3. Blockade of flk-1 suppressed MCP-1 induction in VSMCs in vivo and ex vivo. Immunostaining of MCP-1 and α-SMA revealed that MCP-1 is induced in the medial VSMCs 3 days after injury (A). Scale indicates 200 μm. VEGF-induced MCP-1 expression in cultured aortas was inhibited by sFlt-1 gene transfer (B, n=3 each) and anti–flk-1 antibody (C, n=3 each). W: wild type mice, F: Flt-1 $TK^{-/-}$ mice.

flt-1, mediates MCP-1 induction in the VSMCs immediately after vascular injury. Next, we examined the role of each VEGF receptor in MCP-1 induction in ex vivo culture model. Mouse aorta was harvested from WT, Flt-1 $TK^{-/-}$, and sFlt-1 plasmid-administrated Flt-1 $TK^{-/-}$ mice. The aortas were stimulated with VEGF (50 ng/mL) after 24-hour starvation, and induction of MCP-1 was quantified by real-time PCR. Real-time PCR showed that VEGF-induced expression of MCP-1, which is partially but not significantly inhibited by Flt-1 TK deletion and is completely inhibited by sFlt-1 gene transfer, suggesting that VEGF-induced MCP-1 mRNA transcription is primarily mediated by flk-1 (Figure 3B). Blockade of each VEGF receptor by neutralizing antibodies showed that anti–flt-1 antibody had no effect; by contrast, anti–flk-1 antibody completely inhibited VEGF-induced MCP-1 expression (Figure 3C). Finally we examined the effect of each VEGF receptor blockade on VEGF-induced MCP-1 expression in mouse aortic VSMCs. Blocking antibody of flt-1 did not inhibit VEGF-induced MCP-1 expression. In contrast, blocking antibody of flk-1 significantly inhibited VEGF-induced MCP-1 expression (supplemental Figure I, please see http://atvb.ahajournals.org). These results suggest that VEGF induces MCP-1 expression by flk-1–mediated mechanisms in mouse VSMCs. We also examined whether blockade of VEGF influences PDGF signaling that may mediate MCP-1 induction in injured arterial wall.[23] In vitro study using cultured VSMCs revealed that blockade of VEGF by sFlt-1 gene transfer or sFlt-1 protein does not

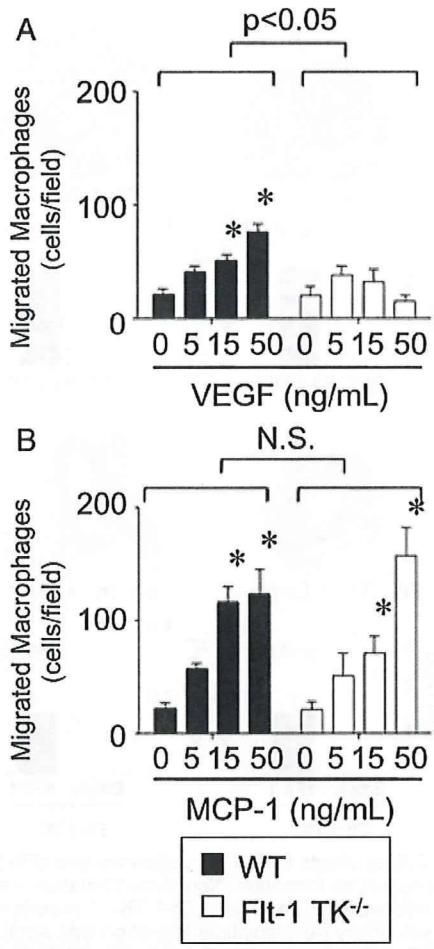

Figure 4. Flt-1 TK deficiency blunted VEGF-induced chemotaxis of macrophages. Chemotaxis of peritoneal macrophage to VEGF or MCP-1 was examined in Boyden chamber experiments. VEGF induced significant chemotaxis in WT mice, which was blunted in Flt-1 $TK^{-/-}$ mice (A). MCP-1 induced prominent and equivalent chemotaxis in WT and Flt-1 $TK^{-/-}$ mice (B). n=6 to 7 for each group. *$P<0.05$ vs control.

inhibit PDGF-induced phosphorylation of PDGF receptors, suggesting that blockade of flk-1 inhibit MCP-1 induction via PDGF-independent mechanisms (supplemental Figure II).

Macrophage Chemotaxis in WT and Flt-1 $TK^{-/-}$ Mice

It is reported that human monocytes exclusively express flt-1 and that VEGF induces chemotaxis by flt-1–mediated mechanism.[13] We performed Boyden chamber experiment to examine macrophage chemotactic function in response to VEGF or MCP-1 in WT and Flt-1 $TK^{-/-}$ mice. VEGF induced significant chemotaxis of peritoneal macrophage from WT mice, which was abolished by Flt-1 TK deficiency (Figure 4A), suggesting that flt-1 essentially mediates VEGF-induced chemotaxis. By contrast, MCP-1 caused more prominent chemotaxis in WT and Flt-1 $TK^{-/-}$ mice equivalently (Figure 4B). These results suggest that MCP-1–induced chemotaxis was preserved in Flt-1 $TK^{-/-}$ mice, and MCP-1 is a primary mediator of flk-1–dependent macrophage recruitment in injured vascular wall even in the Flt-1 TK deficiency.